



1 **Quantifying spatiotemporal variability in zooplankton dynamics in the Gulf of Mexico with**  
2 **a physical-biogeochemical model**

3

4 Taylor A Shropshire<sup>1,2</sup>, Steven L Morey<sup>3</sup>, Eric P Chassignet<sup>1,2</sup>, Alexandra Bozec<sup>1,2</sup>, Victoria J  
5 Coles<sup>4</sup>, Michael R Landry<sup>5</sup>, Rasmus Swalethorp<sup>5</sup>, Glenn Zapfe<sup>6</sup>, Michael R Stukel<sup>1,2</sup>

6

7 <sup>1</sup>Department of Earth Ocean and Atmospheric Sciences, Florida State University, Tallahassee, FL 32303

8 <sup>2</sup>Center for Ocean-Atmospheric Prediction Studies, Florida State University, Tallahassee, FL

9 <sup>3</sup>School of the Environment, Florida A&M University, Tallahassee, FL

10 <sup>4</sup>University of Maryland Center for Environmental Science, PO Box 775 Cambridge MD 21613

11 <sup>5</sup>Integrative Oceanography Division, Scripps Institution of Oceanography, 8622 Kennel Way, La Jolla, CA 92037

12 <sup>6</sup>University of Southern Mississippi, Division of Coastal Sciences, Hattiesburg, MS, 39406

13

14 Correspondence: Taylor A. Shropshire (tshropshire@fsu.edu)



16 **Abstract**

17 Zooplankton play an important role in global biogeochemistry and their secondary production  
18 supports valuable fisheries of the world's oceans. Currently, zooplankton abundances cannot be  
19 estimated using remote sensing techniques. Hence, coupled physical-biogeochemical models  
20 (PBMs) provide an important tool for studying zooplankton on regional and global scales.  
21 However, evaluating the accuracy of zooplankton abundance estimates from PBMs has been a  
22 major challenge as a result of sparse observations. In this study, we configure a PBM for the Gulf  
23 of Mexico (GoM) from 1993-2012 and validate the model against an extensive combination of in  
24 situ biomass and rate measurements including total mesozooplankton biomass, size-fractionated  
25 mesozooplankton biomass and grazing rates, microzooplankton specific grazing rates, surface  
26 chlorophyll, deep chlorophyll maximum depth, phytoplankton specific growth rates, and net  
27 primary production. Spatial variability in mesozooplankton biomass climatology observed in a  
28 multi-decadal database for the northern GoM is well resolved by the model with a statistically  
29 significant ( $p < 0.01$ ) correlation of 0.90. Mesozooplankton secondary production for the region  
30 averaged  $66 \pm 8$  mt C yr<sup>-1</sup> equivalent to approximately 10% of NPP and ranged from 51 to 82 mt  
31 C yr<sup>-1</sup>. In terms of diet, model results from the shelf regions suggest that herbivory is the dominant  
32 feeding mode for small mesozooplankton (<1-mm) whereas larger mesozooplankton are primarily  
33 carnivorous. However, in open-ocean, oligotrophic regions, both groups of mesozooplankton have  
34 proportionally greater reliance on heterotrophic protists as a food source. This highlights the  
35 important role of microbial and protistan food webs in sustaining mesozooplankton biomass in the  
36 GoM which serves as the primary food source for early life stages of many commercially-  
37 important fish species, including tuna.



## 38 1. Introduction

39 Within marine pelagic ecosystems zooplankton function as an important energy pathway between  
40 the base of the food chain and higher trophic levels such as fish, birds, and mammals (Landry et  
41 al., 2019; Mitra et al., 2014). Zooplankton also have a well-documented impact on chemical  
42 cycling in the ocean (Buitenhuis et al., 2006; Steinberg and Landry, 2017; Turner, 2015). The  
43 ecological roles of zooplankton, however, are varied and taxon-dependent. Globally, protistan  
44 grazing is the largest source of phytoplankton mortality, accounting for 67% of daily  
45 phytoplankton growth (Landry and Calbet, 2004). Protistan zooplankton function primarily within  
46 the microbial loop leading to efficient nutrient regeneration in the surface ocean (Sherr and Sherr,  
47 2002; Strom et al., 1997). By contrast, mesozooplankton contribute significantly less to  
48 phytoplankton grazing pressure consuming an estimated 12% of primary production (PP) globally  
49 (Calbet, 2001) yet strongly impact the biological carbon pump. In addition to top-down grazing  
50 pressure on phytoplankton, mesozooplankton impact the biological carbon pump through  
51 production of sinking fecal pellets, consumption of sinking particles and active carbon transport  
52 during diel vertical migration (Steinberg and Landry, 2017; Turner, 2015). While contributing  
53 notably less to phytoplankton grazing pressure than protists, herbivorous mesozooplankton are  
54 important to study as they are often associated with shorter food chains that enable efficient energy  
55 transfer from primary producers to higher trophic levels of particular societal interest such as  
56 economically valuable fish species and/or their planktonic larvae.

57 Zooplankton populations have been identified as being vulnerable to impacts of a warming ocean  
58 (Caron and Hutchins, 2013; Pörtner and Farrell, 2008; Straile, 1997), through both impacts of  
59 temperature on metabolic rates (Ikeda et al., 2001; Kjellerup et al., 2012) and thermal stratification-  
60 driven alterations in food web structure (Landry et al., 2019; Richardson, 2008). Studies aimed at  
61 monitoring and predicting zooplankton populations are therefore critical to understanding the first-  
62 order effects of a warming ocean on marine ecosystems given the importance of secondary  
63 production and the impact zooplankton have on biogeochemical cycling. Despite their importance,  
64 historically zooplankton have been sampled with limited temporal and spatial resolution. While  
65 remote sensing has provided an enormous advancement in observing ocean hydrodynamics and  
66 phytoplankton variability, zooplankton abundance cannot currently be estimated from space. Thus  
67 numerical models provide a unique oceanographic research tool for studying zooplankton on basin  
68 and global scales (Buitenhuis et al., 2006; Sailley et al., 2013; Werner et al., 2007). Evaluating the



69 accuracy of zooplankton abundance estimates from numerical models, such as three-dimensional  
70 physical-biogeochemical ocean models (PBMs), has been a major challenge in previous modeling  
71 studies as a result of sparse ship-based observations in most regions (Everett et al., 2017).  
72 Consequently, zooplankton dynamics have been under studied and under validated in PBMs.  
73 Instead, PBMs are typically validated predominately against surface chlorophyll (Chl) from  
74 remote sensing (Doney et al., 2009; Gregg et al., 2003; Xue et al., 2013).

75 In most marine environments, phytoplankton net growth rates and hence biomass are determined  
76 primarily by the imbalance between phytoplankton growth and zooplankton grazing (Landry et  
77 al., 2009). PBMs can accurately predict phytoplankton standing stock (i.e. compare well with  
78 satellite Chl observations) despite being driven by the wrong underlying dynamics leading to major  
79 errors in model estimates of secondary production and nutrient cycling (Anderson, 2005; Franks,  
80 2009). For instance, parameter tuning using only surface Chl as a validation metric can allow broad  
81 patterns in phytoplankton biomass to be reproduced even with gross over- or underestimation of  
82 phytoplankton turnover times. Similarly, even a model that is validated against satellite Chl and  
83 net primary production might completely misrepresent the proportion of phytoplankton mortality  
84 mediated by zooplankton groups, leading to inaccurate estimates of secondary production. Hence,  
85 validating PBMs against zooplankton dynamics is key to increasing confidence in model solutions.  
86 The importance of this validation is further witnessed when considering the impact zooplankton  
87 have on the behavior of biogeochemical models (Everett et al., 2017). Differences in simulated  
88 zooplankton communities expressed through the number of functional types, various mathematical  
89 grazing functional responses, and the arrangement of transfer linkages have been shown to have  
90 substantial impacts on simple and complex biogeochemical model solutions (Gentleman et al.,  
91 2003; Gentleman and Neuheimer, 2008; Mitra et al., 2014; Murray and Parslow, 1999; Saille et  
92 al., 2013).

93 The Gulf of Mexico (GoM) is a particularly suitable study region for examining zooplankton  
94 dynamics with PBMs. In the northern and central Gulf, zooplankton abundance has been  
95 extensively measured for over three decades (1982-present) by the Southeast Area Monitoring and  
96 Assessment Program (SEAMAP). Within the SEAMAP dataset, measured zooplankton abundance  
97 exhibits strong spatiotemporal variability, due to complex physical circulation features within the  
98 GoM. The circulation in regions off the shelf is characterized by substantial upper layer mesoscale



99 activity driven primarily by the energetic Loop Current (Forristall et al., 1992; Maul and Vukovich,  
100 1993; Oey et al., 2005). In contrast, coastal and shelf circulation patterns are predominantly wind-  
101 driven (Morey et al., 2003a, 2013). Freshwater discharged by the Mississippi River and other  
102 smaller rivers is frequently entrained offshore by shelf break interaction with mesoscale features  
103 (e.g., anti-cyclonic loop current eddies), leading to strong horizontal and vertical gradients in  
104 physical and biogeochemical quantities (Morey et al., 2003b). These gradients overlap with the  
105 SEAMAP study region resulting in zooplankton biomass sample collection across  
106 biogeochemically heterogeneous and “patchy” environments which provides a powerful model  
107 constraint. For instance, Chl can range across approximately three orders-of-magnitude ( $\sim 0.01 -$   
108  $10 \text{ mg Chl m}^{-3}$ ) from oligotrophic to eutrophic waters. Similarly, mesozooplankton ( $\geq 202 \mu\text{m}$ )  
109 biomass is highly variable ranging from  $0.1 - 160 \text{ mg C m}^{-3}$  in the SEAMAP dataset.

110 Several PBM studies have been conducted in the GoM, all primarily examining nutrient and  
111 phytoplankton dynamics. Early work by Fennel et al. (2011) examined phytoplankton dynamics  
112 on the Louisiana and Texas continental shelf, concluding that loss terms (e.g., grazing) rather than  
113 growth rates dictated accumulation rates of phytoplankton biomass. With the same biogeochemical  
114 model, Xue et al. (2013) conducted the first gulf-wide PBM study to investigate broad seasonal  
115 biogeochemical variability and used the model to constrain a nitrogen budget for the shelf. More  
116 recently, Gomez et al. (2018) implemented a biogeochemical model with multiple phytoplankton  
117 and zooplankton functional types to gain a more detailed understanding of nutrient limitation and  
118 phytoplankton dynamics in the GoM. To examine phytoplankton seasonality and biogeography in  
119 the oligotrophic Gulf, Damien et al. (2018) validated a PBM based on a unique subsurface  
120 autonomous glider dataset. Together, these studies have demonstrated the utility of PBMs for  
121 investigating the GoM lower trophic level and have also highlighted the key role zooplankton play  
122 in the ecosystem. Specifically, both Fennel et al. (2011) and Gomez et al. (2018) identified the  
123 importance of zooplankton in modulating the simulated seasonal patterns of phytoplankton  
124 biomass, emphasizing the importance of top-down control on the shelf. Although results on the  
125 simulated zooplankton community were not presented, Damien et al. (2018) noted that biotic  
126 processes such as grazing pressure, are “essential to fully understanding the functioning of the  
127 GoM ecosystem.” However, in these studies zooplankton validation is largely absent.



128 In this study, we configured a PBM for the GoM to estimate zooplankton abundance and analyze  
129 zooplankton community dynamics. The PBM is forced by three-dimensional hydrodynamic fields  
130 from a data assimilative Hybrid Coordinate Ocean Model (HYCOM) hindcast of the GoM  
131 (<http://www.hycom.org>). The PBM is based on the biogeochemical model NEMURO (North  
132 Pacific Ecosystem Model for Understanding Regional Oceanography; Kishi et al., 2007), which is  
133 substantially modified here for application to the GoM. The model is integrated over 20-years  
134 (1993-2012) and validated extensively against a combination of remote and in situ measurements  
135 including total mesozooplankton biomass, size-fractionated mesozooplankton biomass and  
136 grazing rates, microzooplankton specific grazing rates, surface Chl, deep Chl maximum depth,  
137 phytoplankton specific growth rates, and net primary production. The goals of this study were to:  
138 1) develop and validate a PBM to estimate mesozooplankton abundance in the GoM, 2)  
139 characterize the spatiotemporal variability in mesozooplankton dietary composition, and 3)  
140 quantify regional mesozooplankton secondary production. We focus primarily on the oligotrophic,  
141 open ocean GoM where prey (i.e. zooplankton) availability may be limiting for fish, their larvae,  
142 and other higher trophic levels.

## 143 **2 Methods and data**

### 144 **2.1 Ocean model framework**

#### 145 **2.1.1 Biogeochemical model description**

146 The biogeochemical model for this study is based on NEMURO (Kishi et al., 2007) but has been  
147 modified and parameterized to more accurately reflect the ecology of the GoM. NEMURO is a  
148 concentration-based lower trophic level ecosystem model originally developed and parameterized  
149 for the North Pacific. Like most marine biogeochemical models, it is structured around simplified  
150 representations of the lower food web originating from earlier nutrient-phytoplankton-zooplankton  
151 models (Fasham et al., 1990; Franks, 2002; Riley, 1946; Steele and Frost, 1977). Complexity is  
152 added through additional state variables and transfer functions with the specific goal of resolving  
153 dynamics within the nutrient, phytoplankton, and zooplankton pools. In total, NEMURO has  
154 eleven state variables: six non-living state variables – nitrate ( $\text{NO}_3$ ), ammonium ( $\text{NH}_4$ ), dissolved  
155 organic nitrogen (DON), particulate organic nitrogen (PON), silicic acid ( $\text{Si}(\text{OH})_4$ ), and particulate  
156 silica (Opal); two phytoplankton state variables – small (SP) and large phytoplankton (LP); and  
157 three zooplankton state variables – small (SZ), large (LZ) and predatory zooplankton (PZ).



158 Each biological state variable in NEMURO is an aggregated representation of taxonomically  
159 diverse plankton groups that function similarly in the ecosystem. The phytoplankton community  
160 in NEMURO is modeled as two functional types of obligate autotrophs: small phytoplankton (SP,  
161 predominantly cyanobacteria and picoeukaryotes in the GoM) and large phytoplankton (LP,  
162 diatoms). Small zooplankton (SZ) represent heterotrophic protists. Metazoan zooplankton are  
163 divided into suspension-feeding mesozooplankton (LZ) and predatory zooplankton (PZ), which  
164 also feed on LP and SZ. Here we assume that LZ and PZ are non-migratory. Heterotrophic bacteria  
165 are implicitly represented in NEMURO by temperature-dependent decomposition rates, which  
166 represent nitrification and remineralization. Sinking in NEMURO is restricted to PON and Opal  
167 pools, and benthic processes are not included. Here, because of the large shelf area in the GoM,  
168 we implemented a simple diagenesis of PON/OP to  $\text{NO}_3/\text{SiO}_4$  and removal of PON/OP through  
169 sedimentation, where 1% of the flux sinking out of bottom cell was removed and 10% converted  
170 back into  $\text{NO}_3/\text{SiO}_4$ . However, we found that this had no significant impact on the model.  
171 NEMURO uses nitrogen as a model “currency” since it is the major limiting macronutrient in  
172 much of the ocean. Silica is also included as a potentially co-limiting nutrient for diatoms. For  
173 more details on the specific processes represented and the interactions between state variables in  
174 NEMURO, we direct readers to Kishi et al. (2007). All model equations are provided in the  
175 Supplement to this manuscript.

176 NEMURO was chosen for the present study because it distinguishes SZ, LZ, and PZ, permitting a  
177 detailed analysis of dynamics within the GoM zooplankton community and allowing for  
178 investigation of multiple zooplankton functional types. In initial GoM simulations, we found that  
179 default NEMURO parameterizations for the North Pacific (Kishi et al., 2007) substantially  
180 overestimated both surface Chl and mesozooplankton biomass relative to observations. To a first  
181 order, we attribute these differences to: 1) substantially higher temperatures in the GoM compared  
182 with the North Pacific, which significantly increase decomposition and growth rates in the model  
183 resulting in higher nutrient recycling and sustained elevated standing stocks of phytoplankton and  
184 zooplankton near the surface, and 2) distinct differences in taxonomic composition of the  
185 phytoplankton and zooplankton communities between the GoM and North Pacific with significant  
186 differences in key parameter values associated with growth and grazing. Justification for each  
187 parameter modification and steps of the model tuning process are outlined in Supplement S2, with



188 a summary of parameter values in **Table S2**. Biogeochemical model forcing, initial, and open  
189 boundary conditions are also outlined in Supplement **S1**.

### 190 **2.1.2 Modifications to the original biogeochemical model**

191 To improve realism for application to the GoM, a total of five structural changes were made to the  
192 original NEMURO transfer functions. First, we removed the SP to LZ grazing pathway. The  
193 original SP state variable for the North Pacific represents nanophytoplankton (e.g.  
194 coccolithophores), which can be important prey of copepods and other mesozooplankton. In the  
195 GoM, however, cyanobacteria and picoeukaryotes (too small for direct feeding by most  
196 mesozooplankton) comprise much of the phytoplankton biomass and hence are represented as SP  
197 in our model. In addition to adding realism, this change in direct trophic connection between SP  
198 and LZ allowed the model to produce a more realistic LP dominated phytoplankton community on  
199 the shelf (see Discussion).

200 Next, quadratic mortality was replaced with linear mortality for all biological state variables with  
201 the exception of predatory zooplankton (PZ). In biogeochemical models, quadratic mortality is  
202 often used for numerical stability and/or to represent implicit loss terms to an un-modeled parasite  
203 or predator that may covary in abundance with its prey (e.g. viral lysis of phytoplankton or  
204 predation by un-modeled higher predators). However, grazing mortality is explicitly modeled in  
205 NEMURO and viral mortality is generally not a substantial loss term for bulk phytoplankton  
206 (Brum et al., 2014; Staniewski and Short, 2018). Quadratic mortality was retained for PZ, to  
207 account for predation pressure of un-modeled planktivorous fish. We found that removal of  
208 quadratic mortality for all other biological state variables led to more realistic mesozooplankton  
209 biomass in the oligotrophic region (see Discussion).

210 The default ammonium inhibition term and light limitation functional form was replaced with a  
211 more widely adopted parameterization. The exponential ammonium inhibition term in the nitrate  
212 limitation function was replaced with the term described by Parker (1993), as has been done in  
213 previous PBM studies (Fennel et al., 2006) due to the non-monotonic behavior of the default  
214 NEMURO ammonium inhibition term. The default light limitation functional form was replaced  
215 with the Platt et al. (1980) functional form that explicitly parameterizes photoinhibition. This  
216 formulation is implemented in newer versions of NEMURO, such as the code used in the Regional



217 Ocean Modeling System (ROMS) NEMURO biogeochemical package. Finally, to account for  
218 photoacclimation and more accurately simulate Deep Chlorophyll Maximum (DCM) dynamics,  
219 we replaced the constant C:Chl parameter with a variable C:Chl module where ratios for SP and  
220 LP were allowed to vary based on the formulation described by Li et al. (2010), which considers  
221 both light and nutrient limitation (see Supplemental). Herein, “default” NEMURO includes the  
222 modified ammonium inhibition, light formulation and variable C:Chl model.

223 In total NEMURO has 75 parameters, 25 of which were modified in the present study. To tune  
224 these parameters, we evaluated the model based on three observational benchmarks: surface Chl  
225 estimated from seaWIFS, depth averaged mesozooplankton biomass from the SEAMAP dataset,  
226 and DCM depth from the SEAMAP dataset. Chl and mesozooplankton biomass were chosen to  
227 evaluate basin scale variability in plankton biomass while the DCM depth was chosen to evaluate  
228 the vertical structure of the simulated ecosystem. We also considered expected patterns of size  
229 structured phytoplankton community composition (i.e. SP:LP ratio), relative magnitudes of total  
230 zooplankton grazing contributions, and the magnitude of loss terms for phytoplankton (grazing,  
231 mortality, respiration, and excretion). Initial model tuning was carried out in an idealized one-  
232 dimensional model before being implemented into the PBM. We outline each parameter change,  
233 justification, and the resulting impact on the ecosystem benchmarks simulated by the one-  
234 dimensional model in Supplement **Table S1**. Where possible, we modified parameters in groups  
235 so that relative changes were consistent throughout the model (e.g. doubling all zooplankton  
236 mortality terms). We also conducted a parameter sensitivity analysis to identify impacts of  
237 parameter changes on the final three-dimensional PBM solution (herein referred to as NEMURO-  
238 GoM) (Section 2.6).

### 239 **2.1.3 Description of the offline numerical environment**

240 To run large numbers of three-dimensional simulations efficiently for basin scale tuning, the  
241 NEMURO-GoM was run offline using the MITgcm offline tracer advection package, which was  
242 selected for this study as it has convenient packages for running offline simulations (McKinley et  
243 al., 2004). That is, the dynamical equations of motion are not computed during the NEMURO-  
244 GoM integration, but rather the physical prognostic variables (i.e., temperature, salinity, and three-  
245 dimensional velocity fields) are prescribed from daily-averaged flow fields saved from a previous  
246 hydrodynamic model integration. This allows the recycled use of flow fields leaving only the tracer



247 equations to be computed. In the offline MITgcm package, the prognostic variables provide input  
248 to an advection scheme and mixing routine that conservatively handles offline advection and  
249 diffusion of the biogeochemical tracer fields. MITgcm has many options for linear and non-linear  
250 advection schemes. Here we use a 3<sup>rd</sup> order direct space time flux limiting scheme. Sub grid-scale  
251 mixing of the biogeochemical fields is handled offline through the nonlocal K-Profile  
252 Parameterization (KPP) package based on mixing schemes developed by Large et al. (1994). For  
253 more information about the MITgcm packages, we direct readers to the MITgcm manual  
254 (<http://mitgcm.org/>).

255 Advantages of running PBMs in an offline environment include: 1) the physical time step in an  
256 offline environment is no longer bound by the dynamical Courant–Friedrichs–Lewy numerical  
257 stability criterion, allowing for longer time steps and fewer iterations; and 2) momentum equations  
258 are not computed during the integration. Instead, the stability of the tracer advection scheme and  
259 time scales needed to resolve biological/physical processes of interest set the limits on the time  
260 steps and prescription frequencies of flow fields. When the physical time step is shorter than the  
261 flow field prescription frequency, a simple linear interpolation of the flow fields is performed  
262 inside the PBM between time steps. It is important to note that offline simulations of tracer  
263 advection have been found to closely resemble online runs (that is, computed together with the  
264 integration of the hydrodynamic model’s prognostic equations) when the three-dimensional flow  
265 fields are prescribed at a frequency that is at or below the inertial period for a region (Hill et al.,  
266 2005).

267 In the present study, the NEMURO-GoM time step (30 minutes) is an order of magnitude greater  
268 than the hydrodynamic model’s (H-GoM, described in Section 2.1.4) baroclinic time step (120  
269 seconds). For reference, the 20-year H-GoM simulation that supplied flow fields for the offline  
270 NEMURO-GoM took a total of ~76 days to run to completion on 64 parallel cores. These time  
271 requirements would increase considerably with the 11 additional biogeochemical tracers used in  
272 NEMURO. In contrast, NEMURO-GoM including the 11 added tracers, ran significantly faster,  
273 taking a total of ~50 h on 80 parallel cores. While computationally advantageous, it is important  
274 to note that offline simulations inherently have greater input and output (I/O) demands that can  
275 become bottlenecks in some applications.



#### 276 **2.1.4 Description of the ocean dynamical fields**

277 The NEMURO-GoM is “forced” by daily averaged three-dimensional velocity, temperature, and  
278 salinity fields from a preexisting 20-year (1993-2012) HYCOM (HYbrid Coordinate Ocean  
279 Model) (Chassignet et al., 2003) regional GoM hindcast (H-GoM). H-GoM is based on version  
280 2.2.99B of the HYCOM code, originally provided by the Naval Oceanographic Office  
281 (NAVOCEANO) Major Shared Resource Center. H-GoM was run at 1/25<sup>th</sup> (~4 km) degree  
282 horizontal resolution with 36 vertical hybrid coordinate layers and assimilated historic, in situ, and  
283 satellite observations. The domain encompasses the entire GoM and extends south of the Mexican-  
284 Cuba Yucatan channel to 18 °N and as far east as 77 °W (**Fig. 1**). Further details on H-GoM  
285 (experiment ID: GOMu0.04/expt\_50.1) including details on model forcing and the main model  
286 configuration file (i.e. blkdat.input\_501) can be found at <https://www.hycom.org>.

287 The H-GoM flow fields were mapped from the HYCOM native vertical coordinate to z-levels used  
288 by the MITgcm. The NEMURO-GoM was configured for 29 vertical z-levels in MITgcm (10-m  
289 intervals from 0-150 m, 25-m intervals from 150-300 m, 50-m intervals from 300-500m, and 1000  
290 m, 2000 m, ~4000 m). Mapping is performed by computing total zonal and meridional transports  
291 across the lateral boundaries of each MITgcm grid cell (e.g., 0-10 m bin; which may include  
292 multiple HYCOM layers) and then dividing by the area of the respective cell face. This vertical  
293 mapping approach is consistent as both HYCOM and MITgcm use an Arakawa C-grid orientation  
294 for model variables. The H-GoM bathymetry was adjusted such that no partial cells existed in the  
295 domain to avoid thin cells. The continuity equation was subsequently used to calculate vertical  
296 velocities. The use of transports in this approach ensures conservation and approximately identical  
297 profiles of vertical velocity to those in H-GoM fields. For mapping of temperature and salinity  
298 fields (used in the KPP mixing routine and for scaling biological temperature dependent rates) a  
299 simple linear interpolation was performed.

300

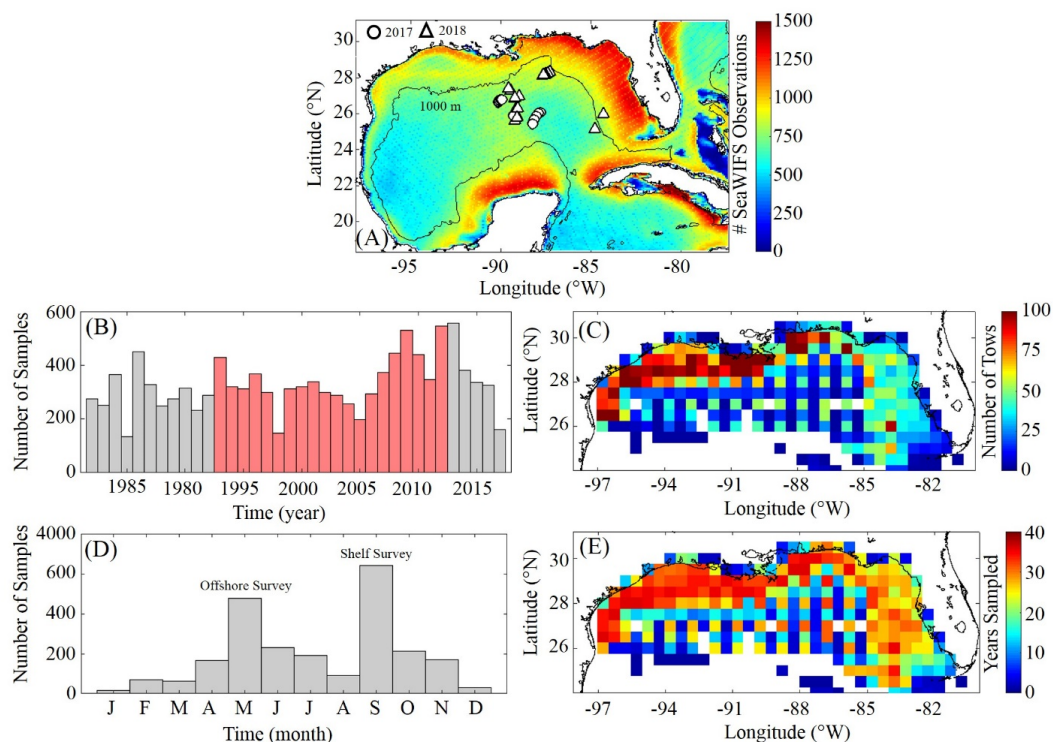
## 301 **2.2 Model validation**

### 302 **2.2.1 SeaWIFS observations used for model validation**

303 A benchmark for surface Chl was determined using the Sea-Viewing Wide Field-of-View Sensor  
304 (SeaWIFS) product from the Ocean Biology Processing Group (OBPG) of the National  
305 Aeronautics and Space Administration (NASA). The product used here is the mapped, level-3,  
306 daily, 9-km resolution product from 4 September 1997 to 10 December 2010 processed according



307 to the algorithm of Hu et al. (2012). To compute model-data point-to-point comparisons, we take  
308 the corresponding daily averaged simulated surface Chl field and interpolate to the SeaWiFS grid  
309 before applying the daily cloud coverage mask corresponding to the matching SeaWiFS image. In  
310 total 4,291 daily images consisting of 22,244,513 non-zero Chl cell values (herein referred to  
311 seaWiFS measurements) were used to validate the PBM. Approximately 500-1200 daily model-  
312 data point-to-point comparisons were made for each SeaWiFS grid cell.



313

314 **Figure 1 (A-E):** Spatial and temporal coverage of all observational data sets used for model  
315 validation. Total number of non-zero SeaWiFS values from the level 3 product from 4 September  
316 1997 to 10 December, 2010 along with cruise sample locations collected during May, 2017  
317 (circles) and 2018 (triangles) (A). Total annual sampling of the SEAMAP surveys from 1983-2017  
318 (B) with samples overlapping with the PBM simulation period denoted in red. Total sample density  
319 within each  $0.5^\circ \times 0.5^\circ$  box (C). Total seasonal sampling (D). Number of years with at least one  
320 sample (E). 1000 m isobaths and coastline are denoted by black continuous lines.



## 321 2.2.2 SEAMAP observations used model validation

322 To evaluate model mesozooplankton biomass estimates, we used zooplankton biomass data  
323 collected during SEAMAP surveys in the northern and central GoM. In total, 11,781 zooplankton  
324 tows were collected from 1983-2017 with two main annual surveys consisting of a spring offshore  
325 and fall shelf sampling grid (**Fig. 1**). These samples were used to generate a climatology which  
326 was used to compare with simulated mesozooplankton climatology. On average, SEAMAP  
327 surveys collected approximately 300 samples per year with a specific sampling array in the  
328 offshore surveys and more general spatial sampling coverage on the shelf. Of these samples, 6,835  
329 were used for direct point-to-point model-data comparisons. Zooplankton biomass samples were  
330 collected using standard gear consisting of a 61 cm diameter bongo frame fitted with two 333  $\mu\text{m}$   
331 mesh nets. This gear is fished in a double-oblique tow pattern from the surface down to 200 m or  
332 5 m off the bottom and back to the surface. During 82 tows in nearshore and oligotrophic regions,  
333 additional samples were collected using a 202  $\mu\text{m}$  mesh net concurrently with the standard 333  $\mu\text{m}$   
334 mesh net. Of these samples roughly half were collected in the oligotrophic GoM. The average ratio  
335 between 333 and 202 samples ( $0.5093 \pm 0.12$ ) was used to convert biomass measurements from  
336 the 333  $\mu\text{m}$  mesh samples so that direct comparisons could be made with simulated  
337 mesozooplankton biomass estimates. In this study we consider SZ size to be  $< 200 \mu\text{m}$ , LZ size to  
338 be 0.2-1 mm, and PZ size to be 1-5 mm. Zooplankton biomasses from SEAMAP surveys were  
339 originally quantified as displacement volumes (DV). Carbon mass (CM) equivalents were  
340 subsequently calculated as  $\log_{10}(\text{CM}) = (\log_{10}(\text{DV}) + 1.434)/0.820$  (Wiebe, 1988; Moriarty and  
341 O'Brien, 2013). CM estimates were converted to model units ( $\text{mmol N m}^{-3}$ ) assuming Redfield  
342 C:N ratio. Simulated mesozooplankton model fields were similarly depth integrated to the bottom  
343 or 200 m to generate the model mesozooplankton biomass climatology or to the sample depth  
344 when performing point-to-point comparisons.

345 Vertical depth profiles of Chl were also approximated at standard stations during SEAMAP  
346 surveys using a SeaBird WETStar pumped fluorometer attached to a CTD. These profiles were  
347 used to determine the depths of the fluorescence maxima, which were then compared directly to  
348 simulated DCM depths at corresponding times and locations. In total, 2,435 profiles were taken  
349 from 2003-2012, with 1,052 profiles overlying bottom depths  $>1000$  m. Profiles were available  
350 for earlier SEAMAP surveys; however, no standard QA/QC protocol for fluorometer data was in



351 place prior to 2003. Model-data agreement for DCM magnitude could not be investigated as the  
352 fluorometer was not calibrated before each cruise.

### 353 **2.2.3 Process rate measurements used for model validation**

354 Although in situ rate measurements are made much less frequently than biological standing stock  
355 measurements, they offer very powerful constraints for validating the internal dynamics of a  
356 biogeochemical model (Franks, 2009). Consequently, we made phytoplankton and zooplankton  
357 rate measurements on two cruises in the open ocean GoM in May 2017 and 2018 and used these  
358 measurements to validate the model (**Fig. 1A**). Since the cruise sampling does not overlap with  
359 our NEMURO-GoM simulation period, we sampled the model at corresponding locations and  
360 times of the year for all 20 years of the simulation to investigate model-data comparisons. On these  
361 cruises, we utilized a quasi-Lagrangian sampling scheme to investigate plankton dynamics in the  
362 oligotrophic GoM. Two drifting arrays (one sediment trap array and one in situ incubation array)  
363 were then deployed to serve as a moving frame of reference during ~4-day studies (“cycles”)  
364 characterizing the water parcel (Landry et al., 2009; Stukel et al., 2015). During these cycles, we  
365 measured daily profiles of Chl, photosynthetically active radiation, phytoplankton growth rates  
366 and productivity, protistan grazing rates, and size-fractionated mesozooplankton biomass and  
367 grazing rates.

368 Protistan grazing rates were measured using the two-point, “mini-dilution” variant of the  
369 microzooplankton grazing dilution method (Landry et al., 1984, 2008; Landry and Hassett, 1982).  
370 Briefly, one 2.8-L polycarbonate bottle was gently filled with whole seawater taken from six  
371 depths (from the surface to the depth of the mixed layer). A second 2.8-L bottle was then filled  
372 with 33% whole seawater and 67% 0.2- $\mu\text{m}$  filtered seawater. Both bottles were then placed in  
373 mesh bags and incubated in situ at natural depths for 24 h. These experiments were conducted on  
374 each day of the ~4-day cycle. After 24 h, the bottles were retrieved, filtered onto glass fiber filters,  
375 and Chl concentrations were determined using the acidification method (Strickland and Parsons.,  
376 1972). Net growth rates ( $k = \ln(\text{Chl}_{\text{final}}/\text{Chl}_{\text{init}})$ ) in each bottle were then determined relative to initial  
377 Chl samples. Phytoplankton specific mortality rates resulting from the grazing pressure of protists  
378 were calculated as  $m = (k_d - k_0)/(1-0.33)$ , where  $k_d$  is the growth rate in the dilute bottle and  $k_0$  is  
379 the growth rate in the control bottle. Phytoplankton specific growth rates were calculated as  $\mu = k_0$   
380 +  $m$ . For additional details, see Landry et al. (2016) and Selph et al. (2016). Phytoplankton net



381 primary production was quantified at the same depths by  $\text{H}^{13}\text{CO}_3^-$  uptake experiments. Triplicate  
382 2.8-L polycarbonate bottles and a fourth “dark” bottle were spiked with  $\text{H}^{13}\text{CO}_3^-$  and incubated in  
383 situ for 24 h at the same sampling depths as for the dilution experiments. Samples were then  
384 filtered, and the  $^{13}\text{C}:^{12}\text{C}$  ratios of particulate matter were determined by isotope ratio mass  
385 spectrometry.

386 Size-fractionated mesozooplankton biomass and grazing rates were determined from daily day-  
387 night paired oblique ring-net tows (1-m diameter, 202- $\mu\text{m}$  mesh) to a depth of 110 m. Upon  
388 recovery, the sample was anesthetized using carbonated water, split using a Folsom splitter,  
389 filtered through a series of nested sieves (5, 2, 1, 0.5, and 0.2 mm), filtered onto preweighed 200-  
390  $\mu\text{m}$  Nitex filters, rinsed with isotonic ammonium formate to remove sea salt, and flash frozen in  
391 liquid nitrogen. In the lab, defrosted samples were weighed for total wet weight, and subsampled  
392 in duplicate (wet weight removed) for gut fluorescence analyses. The remaining wet sample was  
393 dried and subsequently reweighed and combusted for CHN analyses to determine total dry weight  
394 and C and N biomasses. Gut fluorescence subsamples were homogenized using a sonicating tip,  
395 extracted in acetone, and measured for Chl and phaeopigments using the acidification method.  
396 The phaeopigment concentrations in the zooplankton guts were the basis for calculated grazing  
397 rates using gut turnover times based on temperature relationships for mixed zooplankton  
398 assemblages. For additional details, see Décima et al. (2011) and Decima et al. (2016).

### 399 **2.3 Description of the parameter sensitivity experiments**

400 After validating the PBM, a parameter sensitivity analysis consisting of 18 numerical experiments  
401 was conducted to evaluate how robust the final model solution was to parameter changes. For  
402 each experiment, the PBM was configured to simulate four years starting in January 2002. This  
403 time period was concurrent with SeaWIFS and SEAMAP sample coverage. Parameter sensitivity  
404 experiments were initialized from our standard NEMURO-GoM run at 1 January 2002. The PBM  
405 with each parameter change(s) was then allowed to spin up for one year. The last three years (i.e.  
406 2003-2005) were subsequently used for the parameter sensitivity analysis. Direct point-to-point  
407 comparisons were made between model estimates and observations at corresponding sample times  
408 and locations during the model integration. In total, 4,646,459 SeaWIFS Chl measurements, 741  
409 SEAMAP mesozooplankton tows, and 481 SEAMAP fluorescence profiles were used to evaluate  
410 model sensitivity. To better capture relative differences between model and observations across



411 coastal and oligotrophic GoM regions, a  $\log_{10}$  transformation was applied to Chl and  
412 mesozooplankton biomass model-data comparisons before calculating Taylor and Target diagram  
413 statistics. Point-to-point model-data comparisons were also made using the 20-year PBM output,  
414 which included all available data (i.e. 22,244,513 SeaWIFS Chl measurements, 6,835 SEAMAP  
415 mesozooplankton tows, and 2,435 SEAMAP fluorescence profiles). Configurations for each  
416 parameter sensitivity experiment are outlined in **Table S3**.

### 417 **3.0 Results**

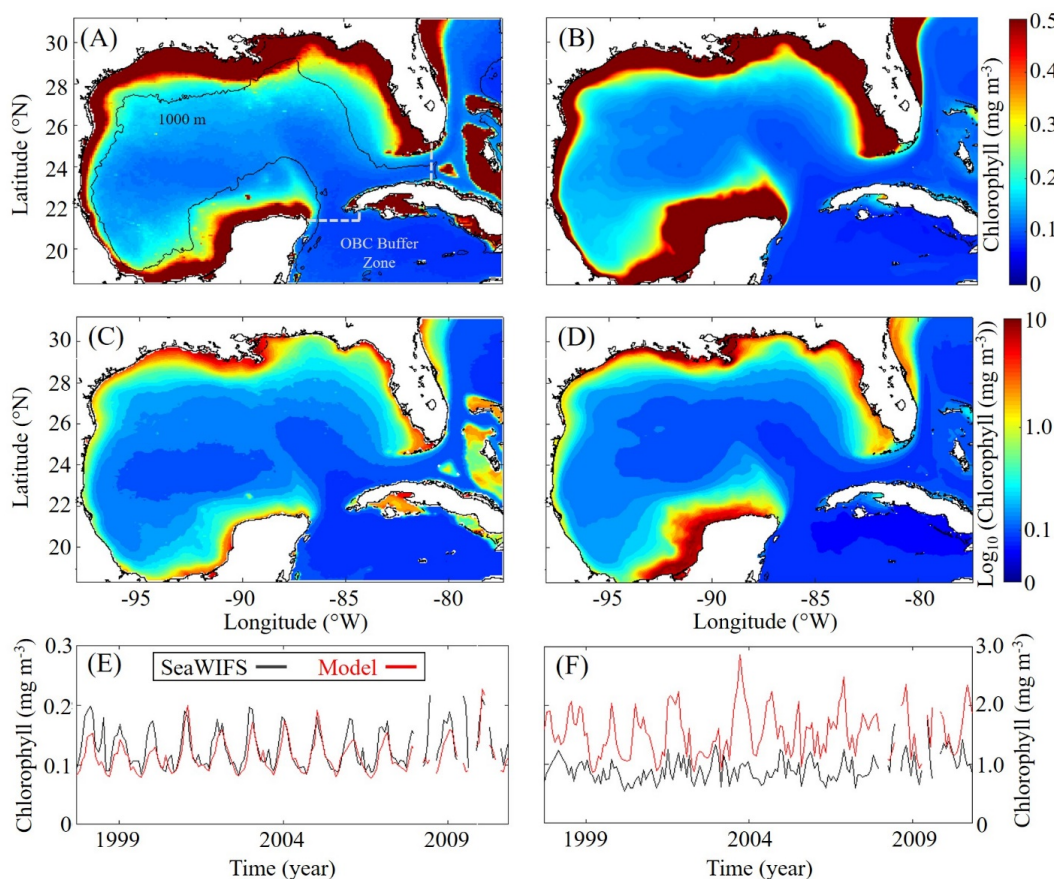
#### 418 **3.1 Regional phytoplankton biomass model-data comparisons**

419 Model surface Chl estimates demonstrate strong agreement with satellite observations (**Fig. 2**).  
420 Spatial covariance between SeaWIFS climatology and model surface Chl climatology (calculated  
421 with daily cloud cover mask applied) is found to be statistically significant ( $p < 0.01$ ) with a  
422 correlation ( $\rho$ ) of 0.72. When model estimates are compared to all 22,244,513 SeaWIFS  
423 measurements at corresponding times and locations (i.e. daily grid cell pairs), we find a  $\rho$  value of  
424 0.50 ( $p < 0.01$ ). To facilitate more detailed model-data comparisons, the GoM domain was divided  
425 into an oligotrophic region ( $\geq 1000$  m bottom depth) and a shelf region ( $< 1000$  m bottom depth).  
426 In the oligotrophic region, the correlation between model-data daily grid cell pairs is significant  
427 but weak ( $\rho = 0.17$ ,  $p < 0.01$ ) as a result of relatively low large-scale spatial variability, and hence  
428 dominance at the mesoscale. However, bias is quite low ( $-0.014$  mg Chl  $m^{-3}$ ) equivalent to 10%  
429 of the observed mean. In the shelf region, the correlation is higher ( $\rho = 0.47$ ,  $p < 0.01$ ) yet the bias  
430 is greater ( $+0.90$  mg Chl  $m^{-3}$ ) equivalent to 92% of the mean. Previous GoM studies have  
431 determined  $\rho$  values based on monthly averages and for reference we calculate them here. Based  
432 on 30-day averages we find a  $\rho$  value of 0.70 ( $p < 0.01$ ) for the oligotrophic region and 0.26 ( $p <$   
433 0.01) for the shelf region.

434 In addition to resolving the dominant spatiotemporal variability, the model also captures the  
435 amplitude of the seasonal surface Chl signal reasonably well. In the oligotrophic region, the model  
436 accurately estimates the observed annual surface Chl minimum (Model:  $0.065 \pm 0.005$  vs.  
437 SeaWIFS:  $0.065 \pm 0.007$  mg Chl  $m^{-3}$ ) while slightly underestimating the observed annual  
438 maximum (Model:  $0.47 \pm 0.15$  vs. SeaWIFS:  $0.75 \pm 0.55$  mg Chl  $m^{-3}$ ). When model estimates for  
439 the entire oligotrophic region are taken into account (i.e. not restricted to satellite measurement  
440 locations and times), we find the annual minimum develops in early September while the annual



441 maximum develops in late January (**Table 1**). In the shelf region, greater model-data mismatch  
442 exists for surface Chl where the model overestimates the observed annual minimum by 15%  
443 (Model:  $0.23 \pm 0.09$  vs. SeaWIFS:  $0.20 \pm 0.07$  mg Chl  $\text{m}^{-3}$ ) and the observed annual maximum by  
444 102% (Model:  $8.09 \pm 1.31$  vs. SeaWIFS:  $4.01 \pm 1.23$  mg Chl  $\text{m}^{-3}$ ). Here, we find the annual surface  
445 Chl seasonal cycle is almost completely out of phase with the oligotrophic region with the annual  
446 minimum developing during early February and the annual maximum developing at the end of  
447 July (**Table 1**).



448

449 **Figure 2 (A-F):** Comparison of surface chlorophyll ( $\text{mg m}^{-3}$ ) between SeaWIFS observations and  
450 model from 4 September 1997 to 10 December 2010. Average SeaWIFS chlorophyll (A). Average  
451 model estimated surface chlorophyll (B).  $\text{Log}_{10}$  of the average SeaWIFS chlorophyll (C).  $\text{Log}_{10}$  of  
452 the average model estimated surface chlorophyll (D). Time series of simulated 30-day average



453 surface chlorophyll (red) and SeaWiFS observations (black) for bottom depths  $\geq 1000$  m (E) and  
 454 bottom depths  $< 1000$  m (F). The 1000 m isobaths and coastline are denoted by black lines.

455 **Table:** Average seasonal minimum and maximum values in the model (1993-2012) and the day  
 456 of year in which they occur for surface chlorophyll ( $\text{mg m}^{-3}$ ), depth integrated phytoplankton  
 457 biomass ( $\text{mg C m}^{-2}$ ), depth integrated net primary production ( $\text{mg C m}^{-2} \text{ d}^{-1}$ ), depth integrated  
 458 mesozooplankton biomass ( $\text{mg C m}^{-2}$ ), and depth integrated mesozooplankton secondary  
 459 production ( $\text{mg C m}^{-2} \text{ d}^{-1}$ ) calculated by spatially averaging daily fields over the oligotrophic  
 460 region (upper half of table) and shelf region (lower half of table). Day of year values are in the  
 461 format “day/month  $\pm$  days.”

	Daily Field Value		Day of Year	
	Annual Min.	Annual Max.	Day of Min.	Day of Max.
Diagnostic (Oligotrophic)				
Surface Chlorophyll	$0.09 \pm 0.005$	$0.27 \pm 0.06$	$9/9 \pm 23$	$1/29 \pm 13$
Phytoplankton Biomass	$2300 \pm 130$	$3600 \pm 140$	$12/26 \pm 7$	$4/29 \pm 17$
Net Primary Production	$290 \pm 70$	$1000 \pm 120$	$12/31 \pm 12$	$7/6 \pm 27$
Mesozooplankton Biomass	$1000 \pm 40$	$1400 \pm 90$	$1/1 \pm 4$	$5/19 \pm 18$
Secondary Production	$18 \pm 4$	$68 \pm 10$	$12/31 \pm 10$	$6/4 \pm 15$
Diagnostic (Shelf)				
Surface Chlorophyll	$1.96 \pm 0.15$	$3.00 \pm 0.30$	$2/8 \pm 37$	$7/31 \pm 58$
Phytoplankton Biomass	$3200 \pm 290$	$5200 \pm 440$	$1/1 \pm 9$	$7/18 \pm 11$
Net Primary Production	$750 \pm 120$	$2000 \pm 220$	$12/31 \pm 8$	$7/21 \pm 14$
Mesozooplankton Biomass	$670 \pm 70$	$1100 \pm 90$	$12/29 \pm 7$	$5/23 \pm 25$
Secondary Production	$94 \pm 17$	$270 \pm 28$	$12/31 \pm 6$	$7/20 \pm 16$

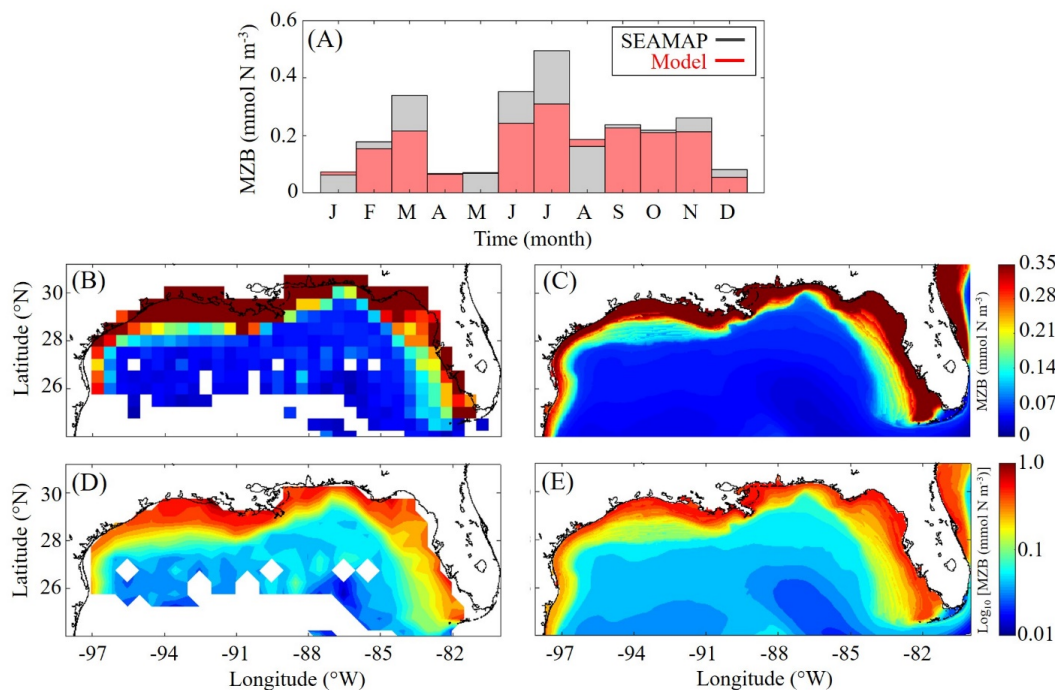
462

463 The model also captures the vertical variability in phytoplankton biomass reasonably well, falling  
 464 within one standard deviation of the observed data. When model estimates of DCM depth are  
 465 compared to all 2,435 SEAMAP CTD casts at corresponding sample times and locations, we find  
 466 a statistically significant correlation ( $\rho = 0.59$ ,  $p < 0.01$ ) with the observed maximum fluorescence  
 467 depth. The observed DCM depth ranged from the surface to 143 m while model values show a  
 468 similar variability ranging from the surface to 163 m. In the oligotrophic region, we find the model  
 469 overestimates the DCM (Model:  $95 \pm 20$  m vs. SEAMAP:  $80 \pm 25$  m) and has a  $\rho$  value of 0.38 ( $p$   
 470  $< 0.01$ ) with a bias of 15 m equivalent to 19% of the observed mean. In the shelf region, the model



471 also overestimates DCM depth (Model:  $63 \pm 26$  m vs. SEAMAP:  $53 \pm 23$  m) and has a  $\rho$  value of  
472 0.49 ( $p < 0.01$ ) with a bias of 10 m equivalent to 19% of the observed mean.

### 473 3.2 Regional zooplankton biomass model-data comparisons



474

475 **Figure 3 (A-E):** Comparison of climatological depth-averaged mesozooplankton biomass (MZB,  
476 mmol N m<sup>-3</sup>) between SEAMAP observations (left) and model output (right). Monthly average  
477 MZB samples organized by month (A). Monthly variability is not representative of seasonality as  
478 sampling locations change between months. MZB from all SEAMAP tows (B). MZB 20-year  
479 model average (C). Log<sub>10</sub> of SEAMAP MZB (D). Log<sub>10</sub> of model MZB (E).

480 Model mesozooplankton biomass (i.e. LZ + PZ) fields compare well with observations in both the  
481 oligotrophic and shelf region (**Fig. 3**). Spatial covariance between SEAMAP climatology and  
482 model climatology of depth-averaged mesozooplankton biomass is statistically significant ( $p <$   
483  $0.01$ ) with a  $\rho$  value of 0.90. When model estimates were compared to SEAMAP tows at  
484 corresponding sample times and locations for the 6,835 measurements overlapping with the  
485 simulation period, the  $\rho$  value is 0.55 ( $p < 0.01$ ). In the oligotrophic region, the model slightly



486 overestimates mesozooplankton biomass (Model:  $4.09 \pm 1.82 \text{ mg C m}^{-3}$  vs. SEAMAP:  $3.52 \pm 3.44$   
487  $\text{mg C m}^{-3}$ ) with  $p$  value of 0.23 ( $p < 0.01$ ) and bias of  $0.57 \text{ mg C m}^{-3}$  equivalent to 16% of the  
488 observed mean. Conversely, in the shelf region the model underestimates mesozooplankton  
489 biomass (Model:  $17.40 \pm 13.58 \text{ mg C m}^{-3}$  vs. SEAMAP:  $20.91 \pm 24.62 \text{ mg C m}^{-3}$ ), with a  $p$  value  
490 of 0.49 ( $p < 0.01$ ) and a bias of  $-3.5 \text{ mg C m}^{-3}$  equivalent to 17% of the observed mean. We note  
491 that model estimates and SEAMAP measurements also compare well with mesozooplankton  
492 biomass measurements (0.2-5 mm) obtained in the oligotrophic region from independent May,  
493 2017 and 2018 cruises (Model:  $5.55 \pm 2.87 \text{ mg C m}^{-3}$  vs. Cruise:  $4.33 \pm 2.28 \text{ mg C m}^{-3}$ ).

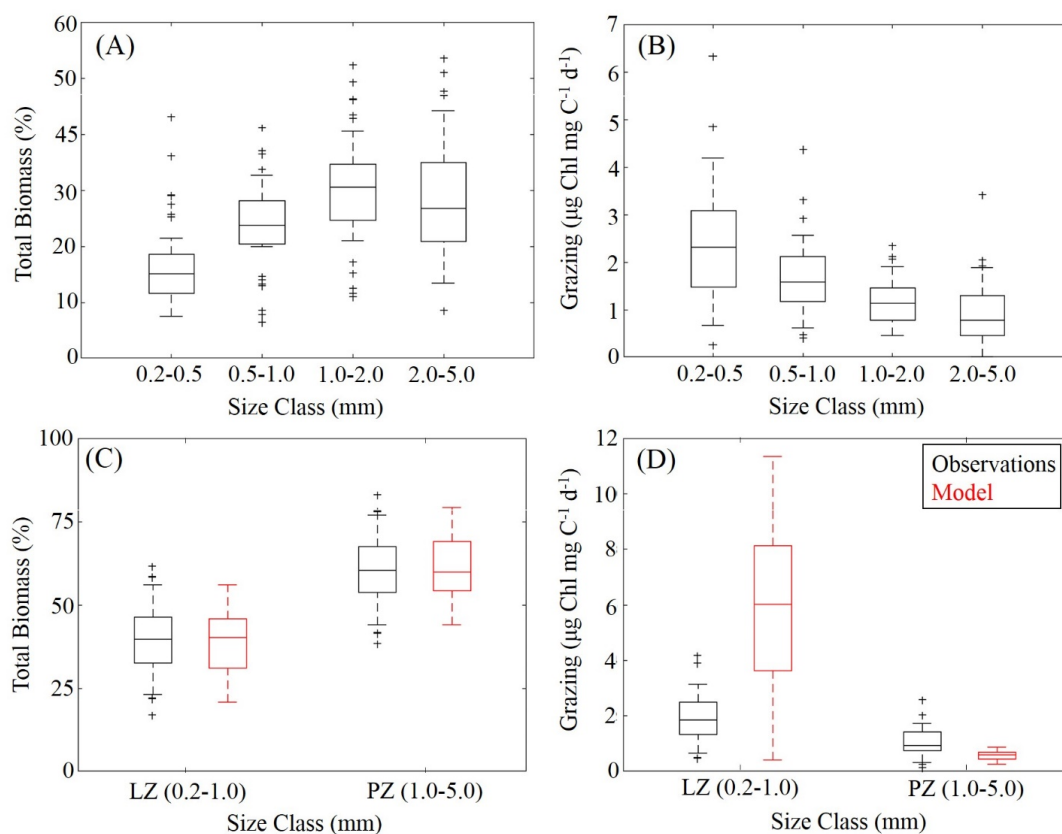
494 Although seasonal cycles in the oligotrophic and shelf regions could not be derived from the  
495 SEAMAP dataset given the significant differences in sampling locations over the course of a year,  
496 we investigated model-data mismatches for each month. We find the model closely matches or  
497 slightly underestimates depth-averaged mesozooplankton biomass throughout most of the year,  
498 with the exception of January, May, and August (**Fig. 3A**). The greatest model-data mismatch  
499 occurs during the months of March, June, July, and December, where the model underestimates  
500 depth-averaged mesozooplankton biomass by approximately 35%. Unlike phytoplankton biomass,  
501 the total mesozooplankton biomass (i.e. depth-integrated) seasonality is similar in both regions of  
502 the GoM. In the oligotrophic region, the annual mesozooplankton biomass minimum (maximum)  
503 develops at the beginning of January (middle of May) while in the shelf region, the annual  
504 minimum (maximum) develops in late December (near the end of May) (**Table 1**).

### 505 **3.3 Phytoplankton growth and zooplankton grazing model-data comparisons**

506 To further constrain the phytoplankton and zooplankton community simulated by the PBM, we  
507 utilized in situ measurements of the planktonic community during Lagrangian process studies  
508 conducted on two cruises in the oligotrophic GoM during May 2017 and 2018. First, we compared  
509 the relative proportions of LZ and PZ biomass to four discrete size classes measured at sea (**Fig.**  
510 **4A, C**). In total, 40 oblique bongo net tows (16 in 2017 and 24 in 2018) sampled the oligotrophic  
511 GoM mesozooplankton community from near surface to a depth ranging from 100 - 135 m. When  
512 the model is sampled yearly corresponding to cruise measurement locations and day of the year,  
513 we find nearly identical size distributions when assuming that LZ approximates the smallest two  
514 size classes of mesozooplankton sampled (“small mesozooplankton”, 0.2-1.0-mm) and PZ  
515 approximates the largest two size classes (“large mesozooplankton”, 1.0-5.0 mm). In both



516 observations and model estimates approximately 40% and 60% of the mesozooplankton  
517 community is composed of LZ and PZ, respectively. In the field data, small mesozooplankton  
518 biomass varied from 33 to 46 % (median = 40%, at 95% C.I.), while model estimates of LZ  
519 biomass vary from 31 to 46% (median = 40%). Large mesozooplankton biomass in the field data  
520 varied from 54 to 67% (median = 60%), while model estimates of PZ biomass vary from 54 to  
521 69% (median = 60%).



522

523 **Figure 4 (A-D):** A summary of field (black) and model (red) estimates of mesozooplankton size-  
524 fractionated biomass and grazing rates. Mesozooplankton size-fractionated biomass as a percent of  
525 total biomass for each of the four size classes measured at sea in May, 2017 and 2018 (A).  
526 Corresponding mesozooplankton specific grazing rates for each of the four size classes (B). Field  
527 data aggregated into two size classes for direct comparison with model biomass estimates for large  
528 (LZ) and predatory (PZ) mesozooplankton (C). Similarly, model data comparison of specific



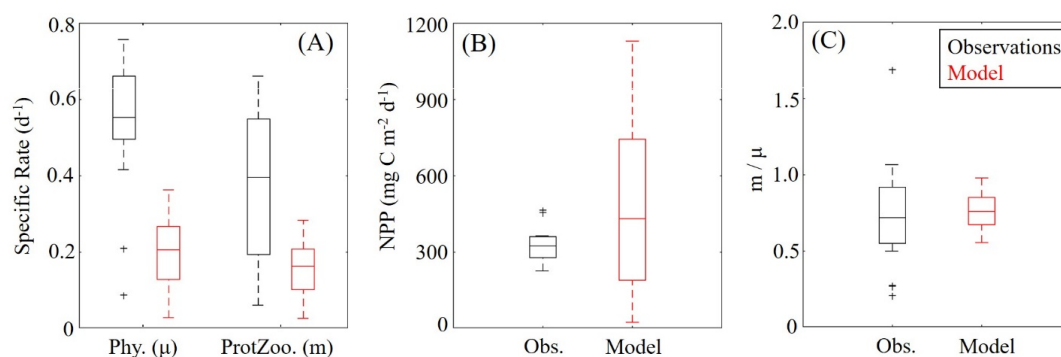
529 grazing rates by large and predatory zooplankton to aggregated field estimates (D). Whiskers  
530 extend to 95% confidence interval. Outliers for model estimates are not shown.

531 We also measured the specific grazing rates of each size class using the gut pigment approach.  
532 Field measurements showed that specific grazing rates consistently decreased with increasing  
533 mesozooplankton size-class (**Fig. 4B**). To compare specific grazing rates in the model to field  
534 measurements ( $\mu\text{g Chl mg C}^{-1} \text{d}^{-1}$ ), we computed grazing on LP by LZ and PZ at each depth.  
535 Grazing terms were converted into units of Chl using the model estimated C:Chl ratio for LP before  
536 being depth-integrated to the corresponding net tow depth and normalized to simulated depth-  
537 integrated LZ and PZ biomasses. We find that model mesozooplankton grazing estimates capture  
538 the general trend of decreased specific grazing rates with increasing mesozooplankton size (**Fig.**  
539 **4D**). However, the model overestimates grazing by small mesozooplankton while underestimating  
540 grazing by large mesozooplankton. In the field data, small mesozooplankton grazing varied from  
541 1.34 to 2.51  $\mu\text{g Chl mg C}^{-1} \text{d}^{-1}$  (median = 1.85) while model estimates of LZ grazing rates vary  
542 from 3.64 to 8.14  $\mu\text{g Chl mg C}^{-1} \text{d}^{-1}$  (median = 6.01). Field measurements of large  
543 mesozooplankton grazing varied from 0.76 to 1.44  $\mu\text{g Chl mg C}^{-1} \text{d}^{-1}$  (median = 0.94), while model  
544 estimates of PZ grazing vary from 0.44 to 0.70  $\mu\text{g Chl mg C}^{-1} \text{d}^{-1}$  (median = 0.58). In terms of total  
545 mesozooplankton grazing, average grazing in the field was found to be  $1.38 \pm 0.59 \mu\text{g Chl mg C}^{-1}$   
546  $\text{d}^{-1}$ , while the model average is  $2.99 \pm 2.20 \mu\text{g Chl mg C}^{-1} \text{d}^{-1}$ . This model-data mismatch likely  
547 results from the fact that, as formulated in NEMURO, LZ and PZ do not necessarily reflect size  
548 classes of mesozooplankton, but rather functional types. In reality, there is substantial overlap  
549 between taxonomic groups with different functional roles and sizes (see Discussion).

550 In addition to measuring the mesozooplankton community, specific phytoplankton growth rates  
551 and specific phytoplankton mortality due to microzooplankton grazing were measured at sea using  
552 the microzooplankton grazing dilution method, and net primary production (NPP) was measured  
553 with  $\text{H}^{13}\text{CO}_3^-$  uptake experiments. We find the model underestimates phytoplankton growth and  
554 microzooplankton grazing while overestimating NPP (**Fig. 5A, B**). This model-data mismatch may  
555 be driven in part by model errors in simulated vertical patterns of phytoplankton growth rates. We  
556 note that model results consistently predict enhanced growth rates at the DCM, while the field  
557 measurements showed surface enhancement of growth rates or relatively constant growth rates  
558 with depth. We believe the collocation of high growth rates at the DCM estimated by the model



559 may reveal a fundamental issue with how biogeochemical models simulated DCM dynamics. This  
560 collocation could explain the lower specific growth rates despite higher NPP we find in the model  
561 (see Discussion).



562

563 **Figure 5 (A-C):** Specific phytoplankton growth ( $\mu$ ,  $d^{-1}$ ) and microzooplankton grazing ( $m$ ,  $d^{-1}$ )  
564 between model (red) and field data (black) (A). Depth-integrated net primary production ( $mg\ C$   
565  $m^{-2}\ d^{-1}$ ) (B). The fraction of phytoplankton growth that is grazed by protists in the model and field  
566 data (C). Whiskers extend to the 95% confidence intervals. Outliers for model estimates are not  
567 shown.

568 Phytoplankton specific growth rates in dilution experiments varied from 0.50 to 0.66  $d^{-1}$  (median  
569 = 0.55  $d^{-1}$ ) while model estimates of phytoplankton (SP+LP) specific growth rates are lower and  
570 vary from 0.13 to 0.27  $d^{-1}$  (median = 0.21  $d^{-1}$ ). In terms of microzooplankton grazing, field data  
571 varied from 0.19 to 0.55  $d^{-1}$  (median = 0.39  $d^{-1}$ ) while model estimates of SZ grazing are also lower  
572 and vary from 0.10 to 0.21  $d^{-1}$  (median = 0.16  $d^{-1}$ ). NPP estimates between model and data show  
573 better agreement where field data varied from 275.61 to 360.09  $mg\ C\ m^{-2}\ d^{-1}$  (median = 321.44  $mg\ C$   
574  $m^{-2}\ d^{-1}$ ) while model estimates vary from 189.75 to 741.04  $mg\ C\ m^{-2}\ d^{-1}$  (median = 430.96  $mg\ C$   
575  $m^{-2}\ d^{-1}$ ). Although we find the model underestimates specific phytoplankton growth and  
576 microzooplankton grazing rates, the relative proportion of NPP being consumed by protists  
577 compares reasonably well to field measurements (**Fig. 5C**). The proportion of NPP grazed in field  
578 data varied from 55% to 92% (median = 72%), while model estimates vary from 67% to 85%  
579 (median = 76%). Notably, the model average proportion of phytoplankton production consumed  
580 by protists closely matches the mean for all tropical waters reported by Calbet & Landry (2004).



581 When specific phytoplankton mortality due to mesozooplankton grazing was calculated at cruise  
582 sample locations, we find that mesozooplankton grazing accounts for  $13 \pm 8 \%$  which also closely  
583 agrees with the global average (Calbet et al., 2001).

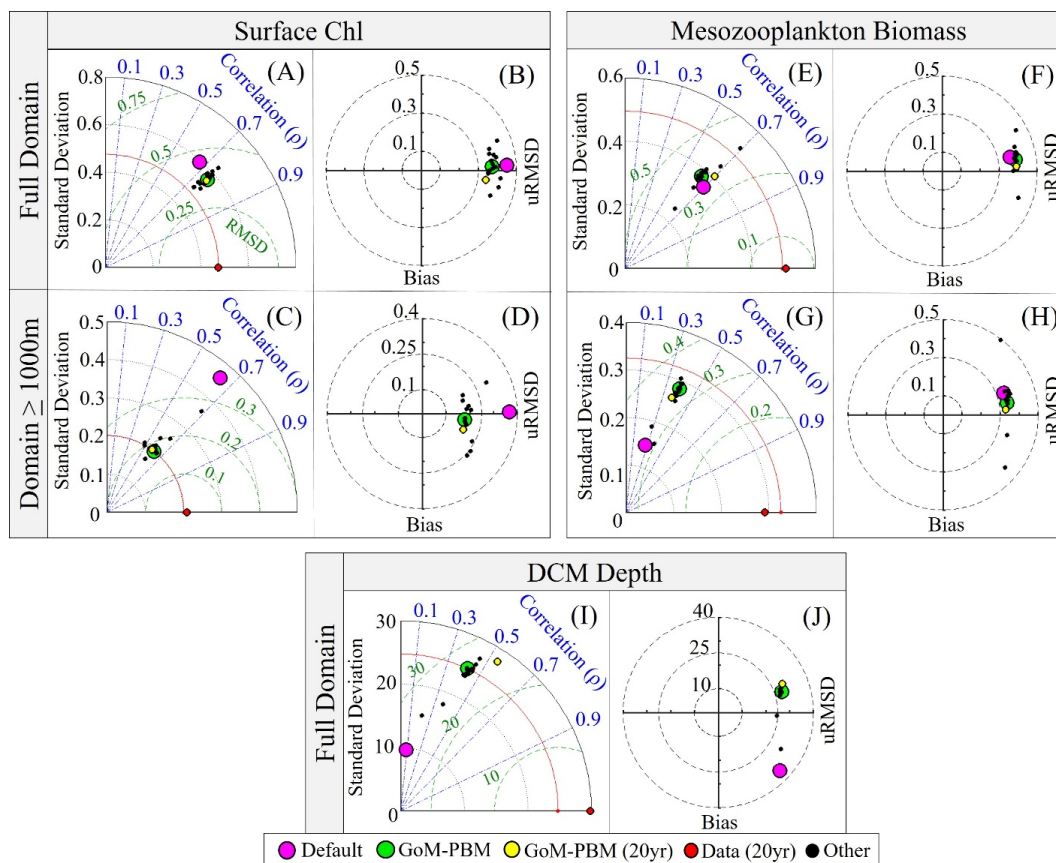
### 584 **3.4 Parameter sensitivity analysis**

585 To evaluate model sensitivity, we investigated the impact of parameter changes on model estimates  
586 over the entire GoM domain and the oligotrophic region, specifically. The separate analysis of the  
587 oligotrophic region was undertaken for two reasons: 1) this region is an area where low  
588 mesozooplankton biomass likely leads to particularly strong prey limitation for fish, their larvae,  
589 and other higher trophic levels and 2) the substantially higher biomass and variability on the shelf  
590 dominates region-wide mean estimates. In comparison to default NEMURO, the NEMURO-GoM  
591 produces estimates of surface Chl, depth averaged mesozooplankton biomass, and DCM depth that  
592 more closely agree with observations (**Fig. 6**). During the parameter sensitivity experiments  
593 SEAMAP observations in the oligotrophic region were almost always located near the Loop  
594 Current which is strongly influenced by the southern open boundary condition. Hence, differences  
595 between simulations were difficult to quantify. Additionally, since mesozooplankton biomass  
596 observations is a depth averaged metric differences between simulations can appear small despite  
597 extreme differences in the vertical distribution of biomass.

598 All parameter sensitivity experiment configurations are outlined in Supplement **Table S3**. Of the  
599 18 sensitivity experiments, the greatest model overestimation of surface Chl occurs when default  
600  $\alpha$  values (slope of the photosynthesis-irradiance curve) are included in NEMURO-GoM (**Fig. 6A-**  
601 **D**). In default NEMURO, SP and LP  $\alpha$  values are an order of magnitude lower (0.01). When default  
602  $\alpha$  values are included in the NEMURO-GoM, they restrict the depth range where phytoplankton  
603 can grow, resulting in substantially shallower DCM depths than observed. Subsequently, the  
604 nitracline becomes unrealistically shallow (~25 m in the oligotrophic region), allowing nutrients  
605 to mix readily into surface water and support higher phytoplankton biomass. The greatest model  
606 underestimation of surface Chl occurs when default quadratic mortality is implemented in the  
607 NEMURO-GoM. Although quadratic mortality tends to increase the lower limit of phytoplankton  
608 biomass, it also increases zooplankton standing stocks which, in this case, allows zooplankton to  
609 graze phytoplankton to unrealistically low levels. We find the exact opposite is true for  
610 mesozooplankton biomass. The greatest overestimation of depth-averaged mesozooplankton



611 biomass occurs when default quadratic mortality is included in the NEMURO-GoM. Conversely,  
 612 when default  $\alpha$  values are included we find the largest underestimation of mesozooplankton  
 613 biomass as a result of low phytoplankton biomass at depth (**Fig. 6E-H**).



614

615 **Figure 6 (A-J):** Taylor and Target diagrams comparing 18 parameter sensitivity experiments  
 616 (black dots) against observations of surface Chl (top left, A-D) depth-averaged mesozooplankton  
 617 biomass (top right, E-H) and deep chlorophyll maximum depth (bottom center, I & J). Each panel  
 618 contains Taylor diagrams (left) and Target diagrams (right). The top two panels are further divided  
 619 based on analysis of all data (top) and with bottom depths  $\geq 1000$  m (bottom). The red arc in Taylor  
 620 diagrams signifies the standard deviation of all observations in the last three years of the four-year  
 621 parameter sensitivity experiments (2002-2006). A  $\log_{10}$  transform is applied to surface chlorophyll  
 622 and depth-averaged mesozooplankton before computing model-data statistics.



623 We also investigated the influence of parameter changes on simulated DCM depth (**Fig. 6I, J**). For  
624 this analysis, we did not isolate the oligotrophic region because average DCM depth does not vary  
625 as substantially as biomass between the shelf and oligotrophic regions (i.e., the shelf does not  
626 dominate the region-wide signal). In contrast to surface Chl and mesozooplankton biomass, default  
627 mortality does not strongly influence DCM depth. However, when default  $\alpha$  values are included,  
628 the model substantially underestimates the actual DCM depth and the standard deviation of DCM  
629 depth as expected. In the NEMURO-GoM, tuned values lead to substantial improvement in DCM  
630 depth, with a standard deviation quite close to observations and a substantially improved  $\rho$  value  
631 (**Fig. 6I**). However, the tuned parameter set results in a small positive bias in DCM depth (i.e.,  
632 deeper than measured DCM by  $\sim 10$  m), although this was less significant than the negative bias in  
633 DCM depth of default NEMURO (i.e., shallower DCM than observations by  $\sim 25$  m).

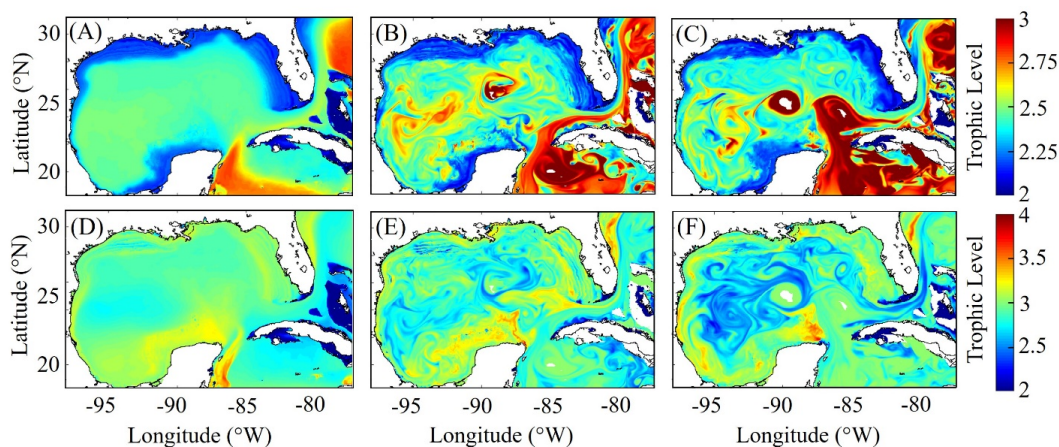
### 634 **3.5 Simulated mesozooplankton diet and secondary production**

635 Trophic level estimates provide a measure of the cumulative diet for mesozooplankton. We  
636 estimated mesozooplankton trophic level in the model by computing the dietary contributions of  
637 each prey in LZ (i.e. LP and SZ) and PZ diets (i.e. LP, SZ, and LZ) while assuming that the trophic  
638 level of LP = 1 and SZ = 2. In the oligotrophic region, both LP and SZ contribute approximately  
639 50% to LZ diet, as indicated by average LZ trophic level near 2.5 ( $2.54 \pm 0.02$ ) (**Fig. 7A**). In the  
640 same region, PZ have a trophic level of  $2.78 \pm 0.04$  indicating a higher contribution of zooplankton  
641 to their diet (i.e. SZ and/or LZ) (**Fig. 7B**). In the shelf region, LZ are more herbivorous, as indicated  
642 by a decrease in trophic level to  $2.31 \pm 0.01$ , while PZ are more carnivorous, as indicated by an  
643 increase in trophic level to  $2.90 \pm 0.04$ .

644 Although there is little evidence in the annual average for LZ diets dominated by zooplankton  
645 (trophic level  $\sim 3$  as commonly found in PZ diets), we commonly find regions in instantaneous  
646 fields during both winter and summer where SZ are the dominant prey source for LZ (**Fig. 7C, E**).  
647 These regions, typically in the Loop Current or Loop Current Eddies (LCEs), highlight the episodic  
648 importance of heterotrophic protists as prey sources for small mesozooplankton in the GoM. High  
649 proportions of SZ in LZ diets can be attributed to the competitive advantage of SP over LP in  
650 extremely low nutrient environments such as in the Loop Current. Instantaneous fields also reveal  
651 that phytoplankton can be an important prey source for PZ as well. This is particularly the case



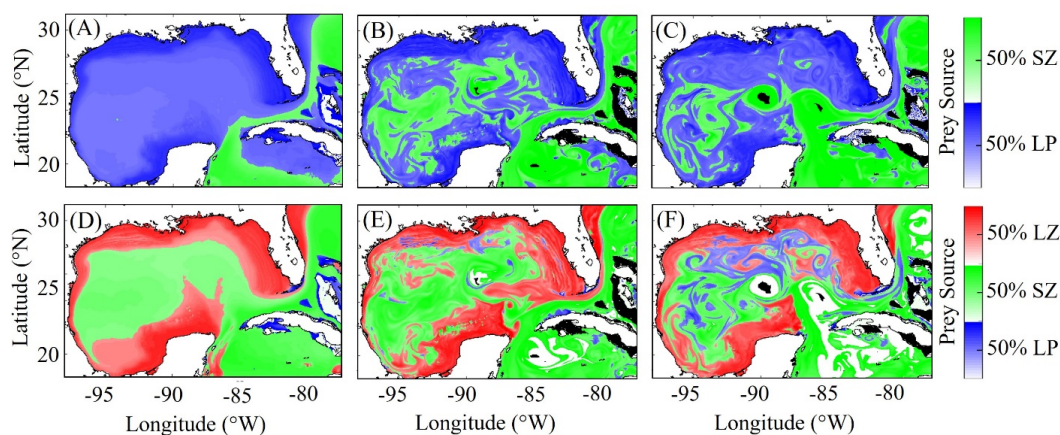
652 during summer, as indicated by trophic levels of around 2.5 in the western oligotrophic GoM (**Fig.**  
653 **7F**).



654

655 **Figure 7 (A-F):** Trophic levels of simulated large zooplankton (LZ, top) and predatory  
656 zooplankton (PZ, bottom). Annual-average trophic positions of LZ (A) and PZ (D). Instantaneous  
657 trophic positions of LZ (B) and PZ (E) for winter conditions on 4 February 2012. Instantaneous  
658 trophic positions of LZ (C) and PZ (F) for summer conditions on 5 August 2011.

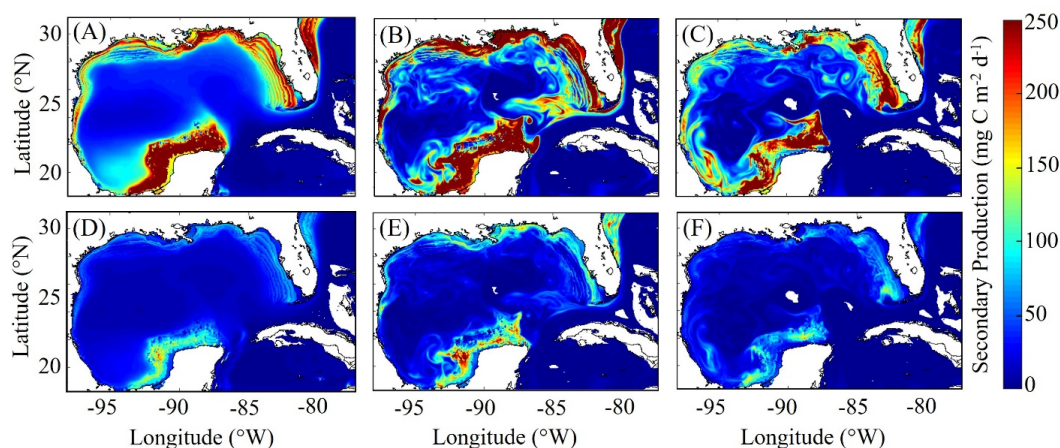
659 In addition to strong variability in trophic positions, there are also regions in the oligotrophic GoM,  
660 most clearly in the centers of LCEs during summer, where the model predicts no feeding by  
661 mesozooplankton (**Fig. 8E**). The convergent anti-cyclonic circulation of LCEs is typically  
662 associated with low phytoplankton biomass, which at times may fall near or below feeding  
663 thresholds in the NEMURO grazing formulation. This formulation is designed to simulate  
664 suppression of feeding activity for zooplankton at mean prey densities that cannot support the  
665 energy expended while searching for prey.



666

667 **Figure 8 (A-F):** Dominant prey source for simulated large zooplankton (LZ, top) and predatory  
668 zooplankton (PZ, bottom). Colors indicate which prey are dominant. Brightness indicates percent  
669 of the dominant prey in the zooplankton diet. Annual averaged field for LZ (A) and PZ (D).  
670 Instantaneous winter condition for LZ (B) and PZ (E) on simulated day 4 February 2012.  
671 Instantaneous summer conditions for LZ (C) and PZ (F) on 4 August 2011.

672 To investigate which prey source contribute the most to LZ and PZ diets, we computed each prey  
673 source term for both LZ and PZ at each grid cell (**Fig. 8**). As we would expect, the dominant prey  
674 source for LZ and PZ closely aligns with the spatial variability in their respective trophic positions.  
675 For LZ diet, herbivory dominates throughout the GoM, except for the Loop Current (**Fig. 8A**). The  
676 LP contribution to LZ diet is highest on the shelf, where LP biomass is also high due to the  
677 competitive advantage LP have over SP in high nutrient conditions. In contrast, PZ diet varies with  
678 the relative availability of SZ and LZ prey. In the oligotrophic region, PZ feed mainly on SZ  
679 (heterotrophic protists), because LZ biomass is relatively low. On the shelf, they consume  
680 primarily LZ (**Fig. 8D**). Despite the significant change in dominant prey between the shelf and  
681 oligotrophic regions, PZ trophic positions remain fairly consistent (**Fig. 7D**) because SZ in the  
682 oligotrophic region and LZ in the shelf region both feed predominantly on phytoplankton. In the  
683 instantaneous fields for winter (**Fig. 8B, E**) and summer (**Fig. 8C, F**), the dominant prey for both  
684 LZ and PZ show substantial mesoscale variability indicating that oceanographic features such as  
685 fronts and eddies influence not only zooplankton biomass but also their ecological roles.



686

687 **Figure 9 (A-F):** Vertically integrated secondary production ( $\text{mg C m}^{-2} \text{d}^{-1}$ ) by simulated large  
688 zooplankton (LZ, top) and predatory zooplankton (PZ, bottom). Annual average of secondary  
689 production for LZ (A) and PZ (D). Instantaneous model output of secondary production in winter  
690 for LZ (B) and PZ (E) on simulated day 4 February 2012. Instantaneous model output for  
691 secondary production in summer for LZ (C) and PZ (F) on 2 August 2011.

692 To our knowledge prior to the current study the regional secondary production for the GoM has  
693 yet to be quantified. In terms of the entire GoM, we find that secondary production averaged  $66 \pm$   
694  $8 \text{ mt C yr}^{-1}$  and ranged from a minimum of  $51 \text{ mt C}$  (in 1999) to a maximum of  $82 \text{ mt C}$  (in 2011).  
695 In the oligotrophic region, LZ secondary production averages  $35 \pm 5 \text{ mg C m}^{-2} \text{d}^{-1}$  while PZ  
696 secondary production is  $11 \pm 2 \text{ mg C m}^{-2} \text{d}^{-1}$  (**Fig. 9**). The annual secondary production minimum  
697 develops at the end of December while the annual maximum develops in the beginning of June  
698 (**Table 1**). In this region, mesozooplankton are responsible for  $14 \pm 2 \text{ mt C yr}^{-1}$ , equivalent to 6%  
699 of NPP. In the shelf region, secondary production is about 4-fold higher, with LZ production of  
700  $146 \pm 17 \text{ mg C m}^{-2} \text{d}^{-1}$  and PZ production of  $42 \pm 5 \text{ mg C m}^{-2} \text{d}^{-1}$ . Here, the annual minimum also  
701 develops at the end of December while the seasonal maximum occurs near the end of July (**Table**  
702 **1**). Secondary production in the shelf region averages  $51 \pm 6 \text{ mt C yr}^{-1}$  and is equivalent to 13% of  
703 NPP.

704 **4 Discussion**



705 Many parameters in biogeochemical models are poorly constrained by observations and laboratory  
706 studies and/or highly variable in the environment. The numbers and uncertainties around these  
707 parameters allow PBMs with varying degrees of tuning to reproduce a single ecosystem attribute  
708 (e.g., surface Chl) even if multiple processes are inaccurately represented (Anderson, 2005;  
709 Franks, 2009). Once validated, one of the main values of coupling physical and biogeochemical  
710 models (i.e. PBMs) is their utility in making inferences about portions of the lower trophic level  
711 that are under sampled and/or difficult to measure in the field. If PBMs are to be utilized for  
712 explaining variability rather than just fitting an observational dataset, multiple ecosystem attributes  
713 must be validated and the underlying model structure and assumptions critically evaluated. In the  
714 section below, we further justify changes to model structure by evaluating the underlying  
715 assumptions in default NEMRUO and discuss model-data mismatch before drawing conclusions  
716 on the GoM zooplankton community and the implications of its dynamics on higher trophic levels.  
717

#### 718 **4.1 Justification for NEMURO modifications**

719 The phytoplankton community in the North Pacific (NP) domain where NEMURO was originally  
720 designed is largely composed of nanoplankton (i.e. original SP) and microplankton (i.e. original  
721 LP). By default, SP are assumed to represent coccolithophores and autotrophic nanoflagellates,  
722 which can be important prey of copepods and other mesozooplankton in temperate and subpolar  
723 regions (Kishi et al., 2007). However, in tropical regions such as the GoM, smaller  
724 picophytoplankton taxa typically dominate particularly in highly oligotrophic regions. Common  
725 picophytoplankton found in the GoM include cyanobacteria and picoeukaryotes which are too  
726 small for most mesozooplankton to feed on. Consequently, the SP to LZ grazing pathway was  
727 removed in the model. We found that removal of this grazing pathway allowed the model to  
728 simulate a more realistic phytoplankton community in the shelf region. Despite intuition, SP  
729 largely dominated the shelf region in the model when LZ were allowed to graze on SP. After closer  
730 inspection we found that grazing of SP sustained LZ biomass on the shelf to levels where top-  
731 down pressure constrained LP standing stocks. This prevented large blooms of LP leading to a  
732 competitive advantage for SP even in highly eutrophic conditions (e.g. near the Mississippi river  
733 delta). We found this was true under a wide range of LP maximum growth rates, LP half saturation  
734 constants, and LZ/PZ grazing rates. Thus, removal of SP to LZ grazing pathway added ecological  
735 realism and improved the model solution.



736 During the model tuning process, we also found that despite a wide range of tested parameter sets  
737 the model (with default quadratic mortality formulation) was unable to simulate mesozooplankton  
738 biomass low enough to match SEAMAP observations in the oligotrophic region. Even with  
739 unrealistically low phytoplankton biomass, equivalent to approximately 50% of surface Chl  
740 observed in SeaWIFS images, the model overestimated mesozooplankton biomass. We found that  
741 to achieve realistic levels of mesozooplankton biomass in the oligotrophic region, default LZ and  
742 PZ mortality parameter values needed to be increased by an order of magnitude. However, this  
743 produced unrealistically high loss rates in the shelf region leading to mesozooplankton biomass  
744 estimates that were substantially lower than SEAMAP shelf observations. Implementation of  
745 linear mortality on all biological state variables (except PZ) resolved this issue by providing the  
746 model with greater dynamic range. In NEMURO, and other biogeochemical models, quadratic  
747 mortality is often used to increase model stability and/or is mechanistically justified as representing  
748 the impact of unmodeled predators that co-vary in abundance with prey (Gentleman and  
749 Neuheimer, 2008; Steele and Henderson, 1992). However, grazing losses of all state variables  
750 (except PZ), are already explicitly modeled in NEMURO by default. Hence, removal of quadratic  
751 mortality also added ecological realism and improved the model solution. Quadratic mortality was  
752 retained for PZ, to account for the implicit predation pressure of un-modeled planktivorous fish.

#### 753 **4.2 Model-data mismatch**

754 The PBM in this study captures a wide range of key regional ecosystem attributes across multiple  
755 trophic levels. Surface Chl estimates were found to agree closely with satellite measurements,  
756 reproducing patterns in both the oligotrophic and shelf region. The latter of which, apart from the  
757 northern shelf, has not been well resolved by previous PBMs (e.g., Gomez et al., 2018; Xue et al.,  
758 2013). The lack of a shelf Chl signature in previous studies may, in some cases, be overly attributed  
759 to bias in satellite measurement due to high concentrations of colored dissolved organic matter on  
760 the shelf. While a clear shelf signature is resolved in the NEMURO-GoM, we find greater model-  
761 data mismatch on the shelf compared to oligotrophic regions. This is an expected finding when  
762 considering the model incorporates climatological river forcing while actual variability is in reality  
763 much more complex. Benthic processes that are not included in the NEMURO-GoM, such as  
764 denitrification (Fennel et al., 2006), may also contribute to model-data discrepancies in the shelf  
765 region.



766 The most noticeable surface Chl model-data mismatch occurs in the southern GoM on the  
767 Campeche Bank (CB) where the model consistently overestimates surface Chl. This  
768 overestimation was also notably present in the PBM implemented by Damien et al. (2018) for the  
769 GoM, particularly in winter. We believe this discrepancy is driven by a combination of error in  
770 the hydrodynamic model associated with overestimation of shelf mixing and simulated nitraclines  
771 that are too shallow, which allows for unrealistic mixing of nitrate into surface waters. Nitrate  
772 profiles from the oligotrophic GoM during May 2017 and 2018 cruises (A. Knapp, pers. comm.)  
773 revealed concentrations are typically below detection limits at depths shallower than 100 m.  
774 However, nitracline depths estimated by the model were shallower than observed with an upper  
775 limit of approximately 80 m (DCM depth was ~100 m) in summer months. While this discrepancy  
776 has minimal impact on average surface Chl over most of the domain, significant model-data  
777 mismatch arises in persistent upwelling areas such as north of the Yucatan Peninsula. In this  
778 region, strong upwelling produces a thin filament of high Chl water that extends northward as  
779 frequently observed in satellite images. To the west, circulation on the CB is characterized by a  
780 westward flow. Together with the shallower simulated nitracline depths, we believe the regional  
781 circulation supplies the CB with excessive nutrient-rich water leading to an overestimation of Chl  
782 by the PBM.

783 We found the model-data mismatch on the CB was reduced in parameter sets that produced  
784 nitracline depths down to 100 m. However, these parameter sets were less realistic in other ways  
785 (e.g. improbably deep DCMs). Given the strong thermal stratification and depth of the nitracline  
786 found in the GoM, we believe nitrogen fixing cyanobacteria may be another important source of  
787 new nitrogen (other than upwelling and mixing) supporting the surface phytoplankton community  
788 in the GoM. In the process of model tuning, we noticed that increasing the DON pool by increasing  
789 the PON to DON decomposition rate was necessary to maintain both relatively deep nitraclines  
790 and realistic surface Chl by providing a slow leeching of ammonium near the surface through  
791 bacterial communities. The need for this slow production of ammonium in surface layers may  
792 reflect the importance of nitrogen fixation, which is not included in NEMURO (Holl et al., 2007;  
793 Mulholland et al., 2006). In future studies including diazotrophs as a separate phytoplankton  
794 functional type would be valuable to investigate the importance of nitrogen fixation in the GoM.



795 Novel to this study, model estimates of mesozooplankton biomass were shown to agree closely  
796 with observations on the shelf and in the oligotrophic GoM. To our knowledge, this study provides  
797 the first quasi regional zooplankton biomass model-data comparisons in the GoM along with the  
798 first model-data comparisons of size-specific zooplankton biomass and grazing rates. Such  
799 comparisons provide the first insights into the potential biases of traditional biogeochemical  
800 models pertaining to zooplankton dynamics (Everett et al., 2017). While the PBM shows broad  
801 agreement with zooplankton observations, some model-data mismatch occurs, particularly for LZ  
802 grazing rates. Some of this discrepancy may arise from temporal sampling issues (rate  
803 measurements were only available for May 2017 and May 2018) or from inaccuracies in the field  
804 grazing measurements. Due to phytodetrital aggregates and *Trichodesmium* colonies in the  
805 zooplankton net tows, our in situ gut pigment measurements were based solely on phaeopigment  
806 content. True grazing rates were likely underestimated because undegraded Chl can be abundant  
807 in the foreguts of zooplankton. An additional source of model-data discrepancy arises from the  
808 fact that the NEMURO model formulation of LZ and PZ does not necessarily reflect a size class  
809 of mesozooplankton, but rather reflects a functional type of mesozooplankton. In reality, there is  
810 overlap between taxonomic groups with different functional roles and different sizes.

811 Since most PBMs focus on validating against satellite-observed surface chlorophyll, the dynamics  
812 of the DCM is often insufficiently investigated. Consequently, many models predict DCM depths  
813 that are far too shallow. Identifying this issue in the literature proved to be difficult seeing that  
814 most studies don't provide profiles of simulated Chl. We note that DCM depths in the DIAZO  
815 model (Stukel et al., 2014) were often quite shallow or completely nonexistent in the portion of  
816 the domain that included the oligotrophic GoM region. Underestimates of DCM depth in the  
817 unmodified COBALT biogeochemical model has also been identified (Moeller et al., 2019). In our  
818 investigation of (Gomez et al., 2018) we found that DCMs in the oligotrophic region were  
819 commonly shallow and weak. In the default NEMURO simulation, DCM depths in the  
820 oligotrophic region were typically at a depth of 25 m, which is much shallower than SEAMAP  
821 observations in the region ( $80 \pm 25$  m). While this issue may seem insignificant, particularly if a  
822 study is focused on mixed-layer dynamics, accurate placement of the DCM can have profound  
823 impacts on PBM behaviors, because the DCM is typically collocated with the nitracline.  
824 Unrealistically shallow DCMs and nitraclines permit unrealistically high nitrate fluxes into the  
825 surface layer following mixing events. Indeed, we believe that a slight underestimation in



826 nitracline depth near the Yucatan Peninsula in our model contributed significantly to the model  
827 overestimation of surface Chl on the Campeche Bank.

828 For these reasons, we devoted substantial effort to tuning phytoplankton dynamics at the DCM.  
829 Modifications to  $\alpha$  (the slope of the photosynthesis-irradiance curve) and attenuation coefficients  
830 allowed us to move the DCM down to realistic depths. However, an additional issue was present  
831 in the default NEMURO simulations, the NEMURO-GoM, and every simulation that we  
832 attempted. In all simulations that formed DCMs, the location of the DCM was always collocated  
833 with a maximum in phytoplankton specific growth rate. However, our field measurements of  
834 phytoplankton growth rates and NPP were either relatively constant with depth or declined in the  
835 DCM. This is not surprising, given the low photon flux at the base of the euphotic zone and the  
836 energetic demands required to upregulate cellular density of light harvesting pigments. However,  
837 in traditional PBMs high biomass DCM cannot form with a low growth rate, because specific  
838 mortality rates tend to co-vary with biomass even if (as in our model) quadratic mortality is not  
839 included.

840 Phytoplankton mortality (in the model and in the observations) is dominated by zooplankton  
841 (particularly protists). Since zooplankton abundance covaries with phytoplankton abundance and  
842 zooplankton specific grazing rates increase with increasing phytoplankton abundance, specific  
843 mortality must co-vary with abundance. This means that phytoplankton mortality rates must be  
844 higher at the DCM biomass peak than in the surface layer and thus a DCM can only be maintained  
845 if growth rates are high. We tested multiple options to try to maintain a DCM with low growth  
846 rates, including using light-dependent grazing formulations (Moeller et al., 2019), but found no  
847 parameterizations that could match the observations. We believe this DCM issue was responsible,  
848 in part, for the overestimates of LZ grazing rates (**Fig. 4D**). The collocation of the biomass and  
849 growth rate maxima also lead to substantial overestimates of production (particularly by LP) at the  
850 DCM, which was then grazed by LZ. Future modeling studies should focus more effort on  
851 dynamics of the DCM.

### 852 **4.3 Mesozooplankton dynamics in the open-ocean oligotrophic Gulf of Mexico**

853 Despite its nutrient-poor conditions, the open-ocean GoM ecosystem is a key region for spawning  
854 and larval development of many commercially important fishes, including Atlantic bluefin tuna,



855 yellowfin tuna, skipjack tuna, sailfish, and mahi mahi (Cornic and Rooker, 2018; Kitchens and  
856 Rooker, 2014; Lindo-Atichati et al., 2012; Muhling et al., 2017; Rooker et al., 2012, 2013). Why  
857 so many species choose such oligotrophic waters as habitat for their larval stages is unknown, but  
858 may be due to reduced predation risk (Bakun, 2013; Bakun and Broad, 2003). Regardless, rapid  
859 growth and survival through the larval period depends on mesozooplankton prey that are suitably  
860 abundant and appropriately sized for these larval fishes. These prey taxa may be especially  
861 sensitive to increased stratification and oligotrophication associated with climate change, making  
862 investigation of their dynamics and production an important topic of research.

863 Mesozooplankton biomass in the oligotrophic GoM was found to be strikingly low in both  
864 observations and PBM estimates with approximately an order of magnitude less biomass in  
865 comparison to the shelf. PBM results clearly show that this low biomass condition arises from  
866 bottom-up resource limitation. Our results suggest that low phytoplankton biomass in oligotrophic  
867 regions, and particularly within Loop Current Eddies, may even lead to localized and episodic  
868 regions where mean concentrations approach thresholds for triggering collapse of  
869 mesozooplankton grazing. Prey limiting conditions for mesozooplankton and their predators  
870 would be expected to occur more frequently in the GoM during warmer ocean conditions. Higher  
871 sea surface temperatures and increased thermal stratification could suppress vertical mixing,  
872 resulting in lower phytoplankton biomass. Indeed, while NEMURO-GoM exhibits severe nutrient  
873 limitation in surface waters, the nitracline in the model is actually weaker and shallower than in  
874 situ measurements during our cruises (A. Knapp, pers. comm.). This suggests potentially greater  
875 nutrient scarcity in surface waters than the model predicts.

876 Despite extreme oligotrophy and dominance of picophytoplankton, our model shows that both PZ  
877 and LZ populations can be sustained at modest abundances in the oligotrophic GoM. Indeed, the  
878 substantial abundances of large (>1-mm) mesozooplankton equivalent to 60% of total  
879 mesozooplankton, as determined by both observations and model results (Fig. 4A, C) is an  
880 important result that helps explain the success of larval fish in the region. Our results show that  
881 large mesozooplankton (PZ) occupy a trophic position of approximately 3.0 in the open ocean  
882 GoM, which is marginally lower than on the shelf where they feed primarily on small  
883 mesozooplankton (LZ). This change in trophic position is associated with a switch from carnivory  
884 to feeding predominantly on heterotrophic protists in the oligotrophic region. This result highlights



885 the importance of intermediate protistan trophic levels in sustaining mesozooplankton  
886 communities in oligotrophic regions. Indeed, both LZ and PZ are found to ingest proportionally  
887 more SZ in the open ocean than on the shelf. Notably, these protistan trophic steps cannot be  
888 quantified by routine field techniques because they have no pigment signature to make them visible  
889 in gut pigment measurements and may not enrich in bulk  $^{15}\text{N}$  leading to isotopic invisibility from  
890 a trophic perspective (Gutiérrez-Rodríguez et al., 2014). Despite their importance, they are also  
891 often missing from GoM ecosystem models (e.g., Fennel et al., 2011) and severely  
892 underrepresented or even absent in complex mass-balance constrained models (Arreguin-Sanchez  
893 et al., 2004; Geers et al., 2016). (Arreguin-Sanchez et al., 2004; Geers et al., 2016). New insights  
894 may arise from focused investigation of phytoplankton→protist→crustacean linkages in  
895 oligotrophic regions in both model and experimental studies. This will likely require the use of  
896 next-generation technologies such as compound specific isotopic analyses of specific amino acids  
897 that have been shown to enrich in protists (Décima et al., 2017) or DNA metabarcoding to assess  
898 zooplankton gut contents (Cleary et al., 2016).

899 Another robust result of our model is the dynamic mesoscale variability in zooplankton abundance,  
900 diet, and trophic position. These results highlight the impact of Loop Current Eddies and  
901 mesoscale fronts and other features in modifying the biogeochemistry and food web of the GoM.  
902 The existence of hot spots of productivity in the GoM has been seen in observational studies (Biggs  
903 and Ressler, 2001), and the importance of GoM mesoscale features to fish larvae has been  
904 hypothesized (Domingues et al., 2016; Lindo-Atichati et al., 2012; Rooker et al., 2012). Our  
905 results suggest that these mesoscale structures may not only modify zooplankton abundances, but  
906 also their trophic roles in the ecosystem, with implications for the transfer efficiencies of carbon  
907 and nitrogen in the pelagic food web.

## 908 **5.0 Conclusions**

909 In this study, we used an extensive suite of in situ measurements to validate zooplankton dynamics  
910 simulated by a PBM of the GoM. The model was able to capture broad patterns in phytoplankton  
911 and mesozooplankton abundances, depth of the deep chlorophyll max, and growth and grazing  
912 patterns. However, a distinct discrepancy was found between vertical profiles of measured and  
913 modeled growth rates of phytoplankton. Despite testing multiple parameterizations for  
914 phytoplankton growth and zooplankton grazing, no model solution was found that could simulate



915 a DCM with high biomass, but low growth rates. Future research is needed to diagnose these  
916 dynamical issues for the DCM. Once validated, the PBM was used to investigate important  
917 characteristics of the GoM mesozooplankton community. Our results suggest that small  
918 mesozooplankton are largely herbivorous and large mesozooplankton largely carnivorous on the  
919 GoM shelf. However, distinct changes in diet were noted in the oligotrophic GoM, where both  
920 groups rely more on protistan prey. Changes in diet and secondary production highlighted in this  
921 study have the potential to impact food availability to higher trophic levels, such as pelagic larval  
922 fishes. In future work, we plan to couple our model to an individual-based model of larval fish to  
923 evaluate the extent to which food resources limit larval fish feeding and growth along their  
924 transport pathways in the GoM. Insights from this ecosystem-based approach may help to better  
925 resolve stock-recruitment relationship that are needed for sustainable fisheries management and  
926 improved stock-assessment models.



927 *Code and data availability.*

928 The model code and model validation data used in this study can be downloaded from GitHub at  
929 <https://github.com/tashrops/NEMURO-GoM>. An idealized one-dimensional version of  
930 NEMURO-GoM written in Matlab is also provided. The three-dimensional NEMURO-GoM  
931 model outputs used in the study are available on the FSU-COAPS server in a Network Common  
932 Data Form (NetCDF format).

933 *Author Contribution.*

934 TAS conducted all numerical simulations and model analysis. EPC, SLM, and AB provided  
935 expertise on the hydrodynamic modeling. MRS and VJC provided expertise on the biogeochemical  
936 model coding and tuning. RS, MRL, and GZ processed and provided data that was central to  
937 NEMURO-GoM's validation. TAS wrote the manuscript with contributions from all authors.

938 *Competing interest.*

939 The authors declare that they have no conflict of interest

940 *Acknowledgements.*

941 We thank the captains and crew of the NOAA ship Nancy Foster and many of our colleagues from  
942 NOAA SEFSC and the NASA-funded Zooplankton from Space project. We thank Oliver Jahn for  
943 providing valuable direction in configuring the offline MITgcm package. We also thank Mandy  
944 Karnauskas and Sang-Ki Lee for their thoughtful advice and guidance on the project. This paper  
945 is a result of research supported by a grant from The Gulf of Mexico Research Initiative under the  
946 CSOMIO project, the National Oceanic and Atmospheric Administration's RESTORE Science  
947 Program under federal funding opportunity NOAA-NOS-NCCOS-2017-2004875, by a NOAA  
948 Fisheries and the Environment grant, and by NASA IDS grant #80NSSC17K0560.



949 **References**

950

951 Anderson, T. R.: Plankton functional type modelling: Running before we can walk?, *J. Plankton*  
952 *Res.*, 27(11), 1073–1081, doi:10.1093/plankt/fbi076, 2005.

953 Arreguin-Sanchez, F., Zetina-Rejón, M., Manickchand-Heileman, S., Ramírez-Rodríguez, M.  
954 and Vidal, L.: Simulated response to harvesting strategies in an exploited ecosystem in the  
955 southwestern Gulf of Mexico, *Ecol. Modell.*, 172(2–4), 421–432,  
956 doi:10.1016/j.ecolmodel.2003.09.016, 2004.

957 Bakun, A.: Ocean eddies, predator pits and bluefin tuna: Implications of an inferred “low risk-  
958 limited payoff” reproductive scheme of a (former) archetypical top predator, *Fish Fish.*, 14(3),  
959 424–438, doi:10.1111/faf.12002, 2013.

960 Bakun, A. and Broad, K.: Environmental “loopholes” and fish population dynamics:  
961 Comparative pattern recognition with focus on El Niño effects in the Pacific, *Fish. Oceanogr.*,  
962 12(4–5), 458–473, doi:10.1046/j.1365-2419.2003.00258.x, 2003.

963 Biggs, D. C. and Ressler, P. H.: Distribution and abundance of phytoplankton, zooplankton,  
964 ichthyoplankton, and micronekton in the deepwater Gulf of Mexico, *Gulf Mex. Sci.*, 2001(1), 7–  
965 29, doi:10.18785/goms.1901.02, 2001.

966 Brum, J.R., Morris, J.J., Décima, M., and Stukel, M.R. (2014). "Mortality in the oceans: Causes  
967 and consequences," in *Eco-DAS IX Symposium Proceedings*, ed. P.F. Kemp. Association for the  
968 Sciences of Limnology and Oceanography), 16-48.

969 Buitenhuis, E., Le Quere, C., Aumont, O., Beaugrand, G., Bunker, A., Hirst, A., Ikeda, T., T, O.  
970 B., Piontkovski, S. and Straile, D.: Biogeochemical fluxes through mesozooplankton - art. no.  
971 GB2003, *Global Biogeochem. Cycles*, 20 (2), NIL\_1-NIL\_18, doi:10.1029/2005GB002511,  
972 2006.

973 Calbet, A.: Mesozooplankton grazing effect on primary production: A global comparative  
974 analysis in marine ecosystems, *Limnol. Oceanogr.*, 46(7), 1824–1830,  
975 doi:10.4319/lo.2001.46.7.1824, 2001.

976 Caron, D. A. and Hutchins, D. A.: The effects of changing climate on microzooplankton grazing  
977 and community structure: Drivers, predictions and knowledge gaps, *J. Plankton Res.*, 35(2), 235–  
978 252, doi:10.1093/plankt/fbs091, 2013.

979 Chassignet, E. P., Smith, L. T., Halliwell, G. R. and Bleck, R.: North Atlantic simulations with  
980 the Hybrid Coordinate Ocean Model (HYCOM): Impact of the vertical coordinate choice,  
981 reference pressure, and thermobaricity, *J. Phys. Oceanogr.*, 33(12), 2504–2526,  
982 doi:10.1175/1520-0485(2003)033<2504:NASWTH>2.0.CO;2, 2003.

983 Cleary, A. C., Durbin, E. G., Rynearson, T. A. and Bailey, J.: Feeding by *Pseudocalanus*  
984 copepods in the Bering Sea: Trophic linkages and a potential mechanism of niche partitioning,  
985 *Deep. Res. Part II Top. Stud. Oceanogr.*, 134, 181–189, doi:10.1016/j.dsr2.2015.04.001, 2016.

986 Cornic, M. and Rooker, J. R.: Influence of oceanographic conditions on the distribution and  
987 abundance of blackfin tuna (*Thunnus atlanticus*) larvae in the Gulf of Mexico, *Fish. Res.*,  
988 201(July 2017), 1–10, doi:10.1016/j.fishres.2017.12.015, 2018.

989 Damien, P., Pasqueron de Fommervault, O., Sheinbaum, J., Jouanno, J., Camacho-Ibar, V. F. and



- 990 Duteil, O.: Partitioning of the Open Waters of the Gulf of Mexico Based on the Seasonal and  
991 Interannual Variability of Chlorophyll Concentration, *J. Geophys. Res. Ocean.*, 123(4), 2592–  
992 2614, doi:10.1002/2017JC013456, 2018.
- 993 Décima, M., Landry, M. R., Stukel, M. R., Lopez-Lopez, L. and Krause, J. W.:  
994 Mesozooplankton biomass and grazing in the Costa Rica Dome: Amplifying variability through  
995 the plankton food web, *J. Plankton Res.*, 38(2), 317–330, doi:10.1093/plankt/fbv091, 2016.
- 996 Décima, M., Landry, M. R. and Rykaczewski, R. R.: Broad scale patterns in mesozooplankton  
997 biomass and grazing in the eastern equatorial Pacific, *Deep. Res. Part II Top. Stud. Oceanogr.*,  
998 58(3–4), 387–399, doi:10.1016/j.dsr.2010.08.006, 2011.
- 999 Décima, M., Landry, M. R., Bradley, C. J. and Fogel, M. L.: Alanine  $\delta^{15}\text{N}$  trophic fractionation  
1000 in heterotrophic protists, *Limnol. Oceanogr.*, 62(5), 2308–2322, doi:10.1002/lno.10567, 2017.
- 1001 Domingues, R., Goni, G., Bringas, F., Muhling, B., Lindo-Atichati, D. and Walter, J.: Variability  
1002 of preferred environmental conditions for Atlantic bluefin tuna (*Thunnus thynnus*) larvae in the  
1003 Gulf of Mexico during 1993–2011, *Fish. Oceanogr.*, 25(3), 320–336, doi:10.1111/fog.12152,  
1004 2016.
- 1005 Doney, S. C., Lima, I., Moore, J. K., Lindsay, K., Behrenfeld, M. J., Westberry, T. K.,  
1006 Mahowald, N., Glover, D. M. and Takahashi, T.: Skill metrics for confronting global upper  
1007 ocean ecosystem-biogeochemistry models against field and remote sensing data, *J. Mar. Syst.*,  
1008 76(1–2), 95–112, doi:10.1016/j.jmarsys.2008.05.015, 2009.
- 1009 Everett, J. D., Baird, M. E., Buchanan, P., Bulman, C., Davies, C., Downie, R., Griffiths, C.,  
1010 Heneghan, R., Kloser, R. J., Laiolo, L., Lara-Lopez, A., Lozano-Montes, H., Matear, R. J.,  
1011 McEnnulty, F., Robson, B., Rochester, W., Skerratt, J., Smith, J. A., Strzelecki, J., Suthers, I. M.,  
1012 Swadling, K. M., van Ruth, P. and Richardson, A. J.: Modeling what we sample and sampling  
1013 what we model: Challenges for zooplankton model assessment, *Front. Mar. Sci.*, 4(MAR), 1–19,  
1014 doi:10.3389/fmars.2017.00077, 2017.
- 1015 Fasham, M. J. R., Ducklow, H. W. and McKelvie, S. M.: A nitrogen-based model of plankton  
1016 dynamics in the ocean mixed layer, *J. Mar. Res.*, 48(3), 591–639, 1990.
- 1017 Fennel, K., Wilkin, J., Levin, J., Moisan, J., O’Reilly, J. and Haidvogel, D.: Nitrogen cycling in  
1018 the Middle Atlantic Bight: Results from a three-dimensional model and implications for the  
1019 North Atlantic nitrogen budget, *Global Biogeochem. Cycles*, 20(3), 1–14,  
1020 doi:10.1029/2005GB002456, 2006.
- 1021 Fennel, K., Hetland, R., Feng, Y. and Dimarco, S.: A coupled physical-biological model of the  
1022 Northern Gulf of Mexico shelf: Model description, validation and analysis of phytoplankton  
1023 variability, *Biogeosciences*, 8(7), 1881–1899, doi:10.5194/bg-8-1881-2011, 2011.
- 1024 Forristall, G. Z., Schaudt, K. J. and Cooper, C. K.: Evolution and kinematics of a loop current  
1025 eddy in the Gulf of Mexico during 1985, *J. Geophys. Res.*, 97(C2), 2173,  
1026 doi:10.1029/91jc02905, 1992.
- 1027 Franks, P. J. S.: NPZ models of plankton dynamics: Their construction, coupling to physics, and  
1028 application, *J. Oceanogr.*, 58(2), 379–387, doi:10.1023/A:1015874028196, 2002.
- 1029 Franks, P. J. S.: Planktonic ecosystem models: Perplexing parameterizations and a failure to fail,  
1030 *J. Plankton Res.*, 31(11), 1299–1306, doi:10.1093/plankt/fbp069, 2009.



- 1031 Geers, T. M., Pikitch, E. K. and Frisk, M. G.: An original model of the northern Gulf of Mexico  
1032 using Ecopath with Ecosim and its implications for the effects of fishing on ecosystem structure  
1033 and maturity, *Deep. Res. Part II Top. Stud. Oceanogr.*, 129, 319–331,  
1034 doi:10.1016/j.dsr2.2014.01.009, 2016.
- 1035 Gentleman, W., Leising, A., Frost, B., Strom, S. and Murray, J.: Functional responses for  
1036 zooplankton feeding on multiple resources: A review of assumptions and biological dynamics,  
1037 *Deep. Res. Part II Top. Stud. Oceanogr.*, 50(22–26), 2847–2875, doi:10.1016/j.dsr2.2003.07.001,  
1038 2003.
- 1039 Gentleman, W. C. and Neuheimer, A. B.: Functional responses and ecosystem dynamics: How  
1040 clearance rates explain the influence of satiation, food-limitation and acclimation, *J. Plankton  
1041 Res.*, 30(11), 1215–1231, doi:10.1093/plankt/fbn078, 2008.
- 1042 Gomez, F. A., Lee, S. K., Liu, Y., Hernandez, F. J., Muller-Karger, F. E. and Lamkin, J. T.:  
1043 Seasonal patterns in phytoplankton biomass across the northern and deep Gulf of Mexico: A  
1044 numerical model study, *Biogeosciences*, 15(11), 3561–3576, doi:10.5194/bg-15-3561-2018,  
1045 2018.
- 1046 Gregg, W. W., Ginoux, P., Schopf, P. S. and Casey, N. W.: Phytoplankton and iron: Validation  
1047 of a global three-dimensional ocean biogeochemical model, *Deep. Res. Part II Top. Stud.  
1048 Oceanogr.*, 50(22–26), 3143–3169, doi:10.1016/j.dsr2.2003.07.013, 2003.
- 1049 Gutiérrez-Rodríguez, A., Décima, M., Popp, B. N. and Landry, M. R.: Isotopic invisibility of  
1050 protozoan trophic steps in marine food webs, *Limnol. Oceanogr.*, 59(5), 1590–1598,  
1051 doi:10.4319/lo.2014.59.5.1590, 2014.
- 1052 Holl, C. M., Waite, A. M., Pesant, S., Thompson, P. A. and Montoya, J. P.: Unicellular  
1053 diazotrophy as a source of nitrogen to Leeuwin Current coastal eddies, *Deep. Res. Part II Top.  
1054 Stud. Oceanogr.*, 54(8–10), 1045–1054, doi:10.1016/j.dsr2.2007.02.002, 2007.
- 1055 Hu, C., Lee, Z. and Franz, B.: Chlorophyll a algorithms for oligotrophic oceans: A novel  
1056 approach based on three-band reflectance difference, *J. Geophys. Res. Ocean.*, 117(1), 1–25,  
1057 doi:10.1029/2011JC007395, 2012.
- 1058 Ikeda, T., Kanno, Y., Ozaki, K. and Shinada, A.: Metabolic rates of epipelagic marine copepods  
1059 as a function of body mass and temperature, *Mar. Biol.*, 139(3), 587–596,  
1060 doi:10.1007/s002270100608, 2001.
- 1061 Kishi, M. J., Kashiwai, M., Ware, D. M., Megrey, B. a., Eslinger, D. L., Werner, F. E., Noguchi-  
1062 Aita, M., Azumaya, T., Fujii, M., Hashimoto, S., Huang, D., Iizumi, H., Ishida, Y., Kang, S.,  
1063 Kantakov, G. a., Kim, H. C., Komatsu, K., Navrotsky, V. V., Smith, S. L., Tadokoro, K., Tsuda,  
1064 A., Yamamura, O., Yamanaka, Y., Yokouchi, K., Yoshie, N., Zhang, J., Zuenko, Y. I. and  
1065 Zvalinsky, V. I.: NEMURO-a lower trophic level model for the North Pacific marine ecosystem,  
1066 *Ecol. Modell.*, 202(1–2), 12–25, doi:10.1016/j.ecolmodel.2006.08.021, 2007.
- 1067 Kitchens, L. L. and Rooker, J. R.: Habitat associations of dolphinfish larvae in the Gulf of  
1068 Mexico, *Fish. Oceanogr.*, 23(6), 460–471, doi:10.1111/fog.12081, 2014.
- 1069 Kjellerup, S., Dünweber, M., Swaethorp, R., Nielsen, T. G., Møller, E. F., Markager, S. and  
1070 Hansen, B. W.: Effects of a future warmer ocean on the coexisting copepods *Calanus  
1071 finmarchicus* and *C. glacialis* in Disko Bay, western Greenland, *Mar. Ecol. Prog. Ser.*, 447, 87–  
1072 108, doi:10.3354/meps09551, 2012.



- 1073 Landry, M., Haas, L. and Fagerness, V.: Dynamics of microbial plankton communities:  
1074 experiments in Kaneohe Bay, Hawaii, *Mar. Ecol. Prog. Ser.*, 16, 127–133,  
1075 doi:10.3354/meps016127, 1984.
- 1076 Landry, M. R. and Calbet, A.: Microzooplankton production in the oceans, *ICES J. Mar. Sci.*,  
1077 61(4), 501–507, doi:10.1016/j.icesjms.2004.03.011, 2004.
- 1078 Landry, M. R. and Hassett, R. P.: Estimating the grazing impact of marine micro-zooplankton,  
1079 *Mar. Biol.*, 67(3), 283–288, doi:10.1007/BF00397668, 1982.
- 1080 Landry, M. R., Decima, M., Simmons, M. P., Hannides, C. C. S. and Daniels, E.:  
1081 Mesozooplankton biomass and grazing responses to Cyclone Opal, a subtropical mesoscale  
1082 eddy, *Deep. Res. Part II Top. Stud. Oceanogr.*, 55(10–13), 1378–1388,  
1083 doi:10.1016/j.dsr2.2008.01.005, 2008.
- 1084 Landry, M. R., Ohman, M. D., Goericke, R., Stukel, M. R. and Tsyrklevich, K.: Lagrangian  
1085 studies of phytoplankton growth and grazing relationships in a coastal upwelling ecosystem off  
1086 Southern California, *Prog. Oceanogr.*, 83(1–4), 208–216, doi:10.1016/j.pocan.2009.07.026,  
1087 2009.
- 1088 Landry, M. R., Selph, K. E., Decima, M., Gutierrez-Rodríguez, A., Stukel, M. R., Taylor, A. G.  
1089 and Pasulka, A. L.: Phytoplankton production and grazing balances in the Costa Rica Dome, *J.*  
1090 *Plankton Res.*, 38(2), 366–379, doi:10.1093/plankt/fbv089, 2016.
- 1091 Landry, M. R., Beckley, L. E. and Muhling, B. A.: Climate sensitivities and uncertainties in  
1092 food-web pathways supporting larval bluefin tuna in subtropical oligotrophic oceans, *ICES J.*  
1093 *Mar. Sci.*, 76(2), 359–369, doi:10.1093/icesjms/fsy184, 2019.
- 1094 Large, W. G., McWilliams, J. C. and Doney, S. C.: Oceanic vertical mixing: A review and a  
1095 model with a nonlocal boundary layer parameterization, *Rev. Geophys.*, 32(4), 363–403,  
1096 doi:10.1029/94RG01872, 1994.
- 1097 Li, Q. P., Franks, P. J. S., Landry, M. R., Goericke, R. and Taylor, A. G.: Modeling  
1098 phytoplankton growth rates and chlorophyll to carbon ratios in California coastal and pelagic  
1099 ecosystems, *J. Geophys. Res. Biogeosciences*, 115(4), 1–12, doi:10.1029/2009JG001111, 2010.
- 1100 Lindo-Atichati, D., Bringas, F., Goni, G., Muhling, B., Muller-Karger, F. E. and Habtes, S.:  
1101 Varying mesoscale structures influence larval fish distribution in the northern Gulf of Mexico,  
1102 *Mar. Ecol. Prog. Ser.*, 463, 245–257, doi:10.3354/meps09860, 2012.
- 1103 Maul, G. A. and Vukovich, F. M.: The Relationship between Variations in the Gulf of Mexico  
1104 Loop Current and Straits of Florida Volume Transport, , 785–796, 1993.
- 1105 McKinley, G. A., Follows, M. J. and Marshall, J.: Mechanisms of air-sea CO<sub>2</sub> flux variability in  
1106 the equatorial Pacific and the North Atlantic, *Global Biogeochem. Cycles*, 18(2), 1–14,  
1107 doi:10.1029/2003GB002179, 2004.
- 1108 Mitra, A., Flynn, K. J., Burkholder, J. M., Berge, T., Calbet, A., Raven, J. A., Granéli, E.,  
1109 Glibert, P. M., Hansen, P. J., Stoecker, D. K., Thingstad, F., Tillmann, U., Våge, S., Wilken, S.  
1110 and Zubkov, M. V.: The role of mixotrophic protists in the biological carbon pump,  
1111 *Biogeosciences*, 11(4), 995–1005, doi:10.5194/bg-11-995-2014, 2014.
- 1112 Moeller, H. V., Laufkötter, C., Sweeney, E. M. and Johnson, M. D.: Light-dependent grazing can  
1113 drive formation and deepening of deep chlorophyll maxima, *Nat. Commun.*, 10(1),



- 1114 doi:10.1038/s41467-019-09591-2, 2019.
- 1115 Morey, S. L., Martin, P. J., O'Brien, J. J., Wallcraft, A. A. and Zavala-Hidalgo, J.: Export  
1116 pathways for river discharged fresh water in the northern Gulf of Mexico, *J. Geophys. Res. C*  
1117 *Ocean.*, 108(10), 1–1, doi:10.1029/2002jc001674, 2003a.
- 1118 Morey, S. L., Schroeder, W. W., O'Brien, J. J. and Zavala-Hidalgo, J.: The annual cycle of  
1119 riverine influence in the eastern Gulf of Mexico basin, *Geophys. Res. Lett.*, 30(16),  
1120 doi:10.1029/2003GL017348, 2003b.
- 1121 Morey, S. L., Zavala-Hidalgo, J. and O'Brien, J. J.: The Seasonal Variability of Continental  
1122 Shelf Circulation in the Northern and Western Gulf of Mexico from a High-Resolution  
1123 Numerical Model, in *Circulation in the Gulf of Mexico: Observations and Models*, vol. 161, pp.  
1124 203–218., 2013.
- 1125 Muhling, B. A., Lamkin, J. T., Alemany, F., García, A., Farley, J., Ingram, G. W., Berastegui, D.  
1126 A., Reglero, P. and Carrion, R. L.: Reproduction and larval biology in tunas, and the importance  
1127 of restricted area spawning grounds., 2017.
- 1128 Mulholland, M. R., Bernhardt, P. W., Heil, C. A., Bronk, D. A. and O'Neil, J. M.: Nitrogen  
1129 fixation and release of fixed nitrogen by *Trichodesmium* spp. in the Gulf of Mexico, *Limnol.*  
1130 *Oceanogr.*, 51(5), 2484, doi:10.4319/lo.2006.51.5.2484, 2006.
- 1131 Murray, A. G. and Parslow, J. S.: The analysis of alternative formulations in a simple model of a  
1132 coastal ecosystem, *Ecol. Modell.*, 119(2–3), 149–166, doi:10.1016/S0304-3800(99)00046-0,  
1133 1999.
- 1134 Oey, L., Ezer, T. and Lee, H.: Loop Current, rings and related circulation in the Gulf of Mexico:  
1135 A review of numerical ..., *Geophys. Monogr. ...*, 161, 31–56 [online] Available from:  
1136 <http://scholar.google.com/scholar?cites=642048877832323420&hl=en#46>, 2005.
- 1137 Parker, R. A.: Dynamic models for ammonium inhibition of nitrate uptake by phytoplankton,  
1138 *Ecol. Modell.*, doi:10.1016/0304-3800(93)90042-Q, 1993.
- 1139 Platt, T., Gallegos, C.L., and Harrison, W.G. (1980). PHOTOINHIBITION OF  
1140 PHOTOSYNTHESIS IN NATURAL ASSEMBLAGES OF MARINE-PHYTOPLANKTON.  
1141 *Journal of Marine Research* 38, 687-701.
- 1142 Pörtner, H. O. and Farrell, A. P.: Physiology and Climate Change *Hans, Science* (80-. ),  
1143 322(October), 690–692 [online] Available from:  
1144 <http://epic.awi.de/epic/Main?puid=32305&lang=en>, 2008.
- 1145 Richardson, A. J.: In hot water: Zooplankton and climate change, *ICES J. Mar. Sci.*, 65(3), 279–  
1146 295, doi:10.1093/icesjms/fsn028, 2008.
- 1147 Riley, G. A.: Factors controlling phytoplankton populations on Georges Bank, *J. Mar. Res.*, 6(1),  
1148 54–73, 1946.
- 1149 Rooker, J. R., Simms, J. R., David Wells, R. J., Holt, S. A., Holt, G. J., Graves, J. E. and Furey,  
1150 N. B.: Distribution and habitat associations of billfish and swordfish larvae across mesoscale  
1151 features in the gulf of Mexico, *PLoS One*, 7(4), doi:10.1371/journal.pone.0034180, 2012.
- 1152 Rooker, J. R., Kitchens, L. L., Dance, M. A., Wells, R. J. D., Falterman, B. and Cornic, M.:  
1153 Spatial, Temporal, and Habitat-Related Variation in Abundance of Pelagic Fishes in the Gulf of



- 1154 Mexico: Potential Implications of the Deepwater Horizon Oil Spill, *PLoS One*, 8(10),  
1155 doi:10.1371/journal.pone.0076080, 2013.
- 1156 Sailley, S. F., Vogt, M., Doney, S. C., Aita, M. N., Bopp, L., Buitenhuis, E. T., Hashioka, T.,  
1157 Lima, I., Le Quéré, C. and Yamanaka, Y.: Comparing food web structures and dynamics across a  
1158 suite of global marine ecosystem models, *Ecol. Modell.*, 261–262, 43–57,  
1159 doi:10.1016/j.ecolmodel.2013.04.006, 2013.
- 1160 Selph, K. E., Landry, M. R., Taylor, A. G., Gutierrez-Rodríguez, A., Stukel, M. R., Wokuluk, J.  
1161 and Pasulka, A.: Phytoplankton production and taxon-specific growth rates in the Costa Rica  
1162 Dome, *J. Plankton Res.*, 38(2), 199–215, doi:10.1093/plankt/fbv063, 2016.
- 1163 Sherr, E. B. and Sherr, B. F.: Significance of predation by protists in aquatic microbial food  
1164 webs, *Antonie van Leeuwenhoek, Int. J. Gen. Mol. Microbiol.*, 81(1–4), 293–308,  
1165 doi:10.1023/A:1020591307260, 2002.
- 1166 Staniewski, M. A. and Short, S. M.: Methodological review and meta-analysis of dilution assays  
1167 for estimates of virus- and grazer-mediated phytoplankton mortality, *Limnol. Oceanogr.*  
1168 *Methods*, 16(10), 649–668, doi:10.1002/lom3.10273, 2018.
- 1169 Steele, J.H., and Frost, B.W. (1977). The structure of plankton communities. *Philosophical*  
1170 *Transactions of the Royal Society B-Biological Sciences* 280, 485-534.
- 1171 Steele, J. H. and Henderson, E. W.: The role of predation in plankton models, *J. Plankton Res.*,  
1172 doi:10.1093/plankt/14.1.157, 1992.
- 1173 Steinberg, D. K. and Landry, M. R.: Zooplankton and the Ocean Carbon Cycle, *Ann. Rev. Mar.*  
1174 *Sci.*, 9(1), 413–444, doi:10.1146/annurev-marine-010814-015924, 2017.
- 1175 Straile, D.: and metazoan efficiencies of protozoan Gross growth on food concentration , and  
1176 their dependence zooplankton group ratio , and taxonomic, *Limnol. Oceanogr.*, 42(6), 1375–  
1177 1385, 1997.
- 1178 Strickland, J. D. H. and Parsons., T. R.: A practical handbook for seawater analysis. Second  
1179 Edition. [online] Available from: <http://www.dfo-mpo.gc.ca/Library/1507.pdf>, 1972.
- 1180 Strom, S. L., Benner, R., Ziegler, S. and Dagg, M. J.: Planktonic grazers are a potentially  
1181 important source of marine dissolved organic carbon, *Limnol. Oceanogr.*, 42(6), 1364–1374,  
1182 doi:10.4319/lo.1997.42.6.1364, 1997.
- 1183 Stukel, M. R., Coles, V. J., Brooks, M. T. and Hood, R. R.: Top-down, bottom-up and physical  
1184 controls on diatom-diazotroph assemblage growth in the Amazon River plume, *Biogeosciences*,  
1185 11(12), 3259–3278, doi:10.5194/bg-11-3259-2014, 2014.
- 1186 Stukel, M. R., Kahru, M., Benitez-Nelson, C. R., Décima, M., Goericke, R., Landry, M. R. and  
1187 Ohman, M. D.: Using Lagrangian-based process studies to test satellite algorithms of vertical  
1188 carbon flux in the eastern North Pacific Ocean, *J. Geophys. Res. Ocean.*, 120(11), 7208–7222,  
1189 doi:10.1002/2015JC011264, 2015.
- 1190 Turner, J. T.: Zooplankton fecal pellets, marine snow, phytodetritus and the ocean’s biological  
1191 pump, *Prog. Oceanogr.*, 130, 205–248, doi:10.1016/j.pocean.2014.08.005, 2015.
- 1192 Werner, F. E., Ito, S. I., Megrey, B. A. and Kishi, M. J.: Synthesis of the NEMURO model  
1193 studies and future directions of marine ecosystem modeling, *Ecol. Modell.*, 202(1–2), 211–223,



- 1194 doi:10.1016/j.ecolmodel.2006.08.019, 2007.
- 1195 Xue, Z., He, R., Fennel, K., Cai, W. J., Lohrenz, S. and Hopkinson, C.: Modeling ocean  
1196 circulation and biogeochemical variability in the Gulf of Mexico, *Biogeosciences*, 10(11), 7219–  
1197 7234, doi:10.5194/bg-10-7219-2013, 2013.
- 1198